Published in final edited form as:

Nat Immunol. 2019 July ; 20(7): 865–878. doi:10.1038/s41590-019-0388-z.

The IRE1 ER stress sensor activates natural killer cell immunity in part by regulating c-Myc

Han Dong[1,2], **Nicholas M. Adams**[3,4], **Yichi Xu**[5], **Jin Cao**[6,7,8], **David S.J. Allan**[9], **James R. Carlyle**[10,11], **Xi Chen**[6,7,8], **Joseph C. Sun**[3,4,12,*], and **Laurie H. Glimcher**[1,2,*]

[1]Department of Cancer Immunology and Virology, Dana-Farber Cancer Institute, Boston, MA 02115, USA

[2]Department of Medicine, and Department of Microbiology and Immunology, Brigham and Women's Hospital, and Harvard Medical School, Boston, MA, 02115, USA.

[3]Immunology Program, Memorial Sloan Kettering Cancer Center, New York, NY 10065, USA

[4]Louis V. Gerstner, Jr. Graduate School of Biomedical Sciences, Memorial Sloan Kettering Cancer Center, New York, NY 10065, USA

[5]Developmental Biology Program, Memorial Sloan Kettering Cancer Center, New York, NY 10065, USA

[6]Department of Molecular and Cellular Biology, Baylor College of Medicine, Houston, Texas 77030, USA

[7]Lester and Sue Smith Breast Center, Baylor College of Medicine, Houston, Texas 77030, USA

[8]Dan L. Duncan Cancer Center, Baylor College of Medicine, Houston, Texas 77030, USA

[9]National Heart Lung and Blood Institute, National Institute of Health. Bethesda, MD 20892, USA

[10]Department of Immunology, University of Toronto, Toronto, Ontario, Canada

[11]Sunnybrook Research Institute, Toronto, Ontario, Canada

[12]Department of Immunology and Microbial Pathogenesis, Weill Cornell Medical College, New York, NY 10065, USA

Abstract

[*]Correspondence to Laurie H. Glimcher (laurie_glimcher@dfci.harvard.edu) or Joseph C. Sun (sunj@mskcc.org).

Author contributions

L.H.G. conceptualized the project, and L.H.G and J.C.S provided supervision. L.H.G., J.C.S, H.D. and N.M.A. designed the experiments. H.D. carried out the experiments, and H.D., L.H.G. and J.C.S. analyzed the data. Y.X. performed the bioinformatics analysis. J.C. did the ChIP experiments and analysis under the supervision of X.C. D.S.J.A. and J.R.C. provided critical reagents. H.D., N.M.A. and Y.X. made the figures. H.D. and N.M.A. wrote the original draft. X.C. proposed key experiments and provided critical feedback on the manuscript. J.C.S. and L.H.G. reviewed and edited the manuscript and figures.

Competing interests

L.H.G. is a former Director of Bristol-Myers Squibb and is currently on the board of directors of and holds equity in GlaxoSmithKline Pharmaceuticals and the Waters Corporation. She chairs the scientific advisory board, is a co-founder of and holds equity in Quentis Therapeutics. She also serves on the scientific advisory boards of Repare Therapeutics, Abro and Kaleido Therapeutics.

Natural killer (NK) cells are critical mediators of host immunity to pathogens. Here, we demonstrate that the ER stress sensor inositol-requiring enzyme 1 (IRE1α) and its substrate transcription factor X-box-binding protein 1 (XBP1) drive NK cell responses against viral infection and tumors *in vivo*. IRE1α-XBP1 were essential for expansion of activated mouse and human NK cells and are situated downstream of the mTOR signaling pathway. Transcriptome and chromatin immunoprecipitation analysis revealed c-Myc as a novel and direct downstream target of XBP1 for regulation of NK cell proliferation. Genetic ablation or pharmaceutical blockade of IRE1α downregulated c-Myc, and NK cells with c-Myc haploinsufficency phenocopied IRE1α-XBP1 deficiency. c-Myc overexpression largely rescued the proliferation defect in IRE1α$^{-/-}$ NK cells. Like c-Myc, IRE1α-XBP1 also promotes oxidative phosphorylation in NK cells. Overall, our study identifies a novel IRE1α-XBP1-cMyc axis in NK cell immunity, providing new insight into host protection against infection and cancer.

Introduction

NK cells are critical mediators of host immunity against malignancies and viral infection[1]. Although extrinsic regulators of NK cell development and function including diverse ligands of key NK cell receptors and proinflammatory cytokines from the microenvironment have been identified[2, 3, 4], we understand relatively little about how NK cells translate these signals into critical effector functions[5, 6]. Furthermore, novel features of NK cells have emerged in recent years, including their ability to undergo clonal proliferation and generate long-lived memory; however, the molecular mechanisms underlying these “adaptive” properties require further characterization. The emerging interest in developing NK cell-based cancer immunotherapy[7] and new vaccine strategies for controlling lethal infectious diseases highlights an urgent need for identifying novel intrinsic regulators of NK cell-mediated immunity.

The activation of ER stress sensor IRE1α and its substrate transcription factor XBP1[89] is a hallmark of ‘professional’ secretory cells that must constitutively deal with a high demand for protein synthesis, folding, and secretion[101112]. This highly evolutionarily conserved signaling pathway is also activated in tumor cells[13] and in myeloid-derived suppressor cells[14], macrophages[15], T cells[16] and dendritic cells[17] in response to external stimuli such as hypoxia, nutrient-deprivation and low pH. However, it is unknown whether NK cell function is driven by IRE1α/-XBP1 signaling, and if so, what specific activities it controls.

To address these questions, we used an IRE1α activation reporter mouse strain to demonstrate that activated NK cells upregulate the IRE1α-XBP1 pathway following exposure to pro-inflammatory cytokines *in vitro* and to viral infection *in vivo*. We use newly-engineered genetic mouse models to identify the IRE1α/XBP1 pathway as a positive cell-intrinsic regulator of NK cell proliferation and expansion during viral infection or lymphopenia, and of NK cell-mediated anti-tumor protection. IRE1α-XBP1 is induced by mTOR and STAT4 signaling pathways in activated NK cells. XBP1 facilitates NK cell expansion in part by directly binding to and activating the c-Myc promoter to upregulate key c-Myc target genes required for NK cell expansion as well as by controlling mitochondrial respiration. This study reveals an unexpected role for the IRE1α/XBP1 pathway and for the transcriptional regulator c-Myc in NK cell-mediated immunity.

Results

Upregulation of the IRE1α/XBP1 pathway in activated NK cells

We tested whether the IRE1α-XBP1 ER Stress Response (or Unfolded Protein Response, UPR) is induced in activated NK cells *in vivo* following mouse cytomegalovirus (MCMV) exposure, where NK cells are critical for infection control[2, 18]. Unbiased transcriptome analysis highlighted ER stress as a top enriched gene ontology (GO) category in MCMV-primed NK cells (Fig. 1a), with rapid upregulation at day 1.5 post infection (PI) (Fig. 1b), accompanied by generation of the active spliced XBP1s RNA, and upregulation of canonical XBP1 target genes (Supplementary Fig. 1a). Consistent with this, transgenic ER stress activated indicator (ERAI) reporter mice[19] revealed minimal IRE1α activation in naïve NK cells, but significantly elevated levels in activated NK cells at day 2 PI that returned to baseline by day 7 PI (Fig. 1b,c) indicating transient activation of this pathway in response to viral infection.

NK cell activation during viral infection occurs when exposed to proinflammatory cytokines including IL-12 and IL-18, and ligation of activating receptors[4, 6, 20, 21]. Consistent with *in vivo* findings, RNA-seq analysis of IL-12 and IL-18 *in vitro* activated NK cells showed robust upregulation of the IRE1α-XBP1 UPR signature, *Xbp1s* induction and activation of canonical XBP1 target genes (Fig. 1d, Supplementary Fig. 1b). Results using the ERAI reporter mouse confirmed IRE1α activity in cytokine-activated NK cells from spleen and bone marrow (BM) (Fig. 1e). Notably. XBP1 activation was also observed in primary human NK cells following IL-12 and IL-18 stimulation *in vitro* (Fig. 1f).

We next identified both Stat4 and the mammalian target of rapamycin (mTOR) as upstream regulators of IRE1α-XBP1 function in infection and in cytokine-activated NK cells. $STAT4^{-/-}$ NK cells displayed reduced *Xbp1* and downstream target gene activation during MCMV infection (Supplementary Fig. 1c), and pharmaceutical blockade of mTOR in NK cells significantly reduced IRE1α activation in response to cytokine stimulation *in vitro* (Supplementary Fig. 1d) consistent with mTOR induction of IRE1α-XBP1 function in liver, other organs and cell types[22, 23, 24]. Thus, IRE1α-XBP1 induction in NK cells is at least partially driven by both STAT4 and mTOR signaling pathways.

The UPR also activates transcription factor Chop (encoded by *Ddit3*), a canonical ER stress marker that mediates ER stress responses. Notably, in contrast to MCMV activation of IRE1α/XBP1 in NK cells, MCMV infection repressed *Ddit3* expression at day 1.5 PI compared to naïve NK cells (Fig. 1b, Supplementary Fig. 1a) as did stimulation with IL-12 and IL-18 *in vitro* (Fig. 1d, Supplementary Fig. 1b). In contrast, NK cells treated with the pharmacologic ER stress inducer tunicamycin increased both *Ddit3* and IRE1α-XBP1 activation. (Supplementary Fig. 2a). Hence, viral infection-driven NK cell activation selectively induces a limited or "non-canonical" UPR restricted to the IRE1α-XBP1 branch.

Intrinsic requirement for IRE1α in NK cell antiviral immunity

To determine whether IRE1α-XBP1 activation in NK cells contributes to host protection against lethal viral infection, we generated mice with specific IRE1α ablation in NK cells (denoted as $IRE1^{NK}$, and IRE1α-deficient NK cells henceforth denoted as $IRE1^{NK}$ cells, Supplementary Fig. 2a–f). MCMV-infected $IRE1^{NK}$ were more susceptible to MCMV infection, with significantly increased viral titers and somewhat reduced overall survival (Fig. 2a,b) than littermate control ($IRE1^{f/f}$) mice (Supplementary Fig. 2a–d,f). These data demonstrate that IRE1α is required for NK cell-mediated antiviral immunity.

Intrinsic requirement for IRE1α-XBP1 in NK cell expansion

Adaptive immune features of NK cells can contribute towards host protection against viral infection[25]. Ly49H-expressing NK cells recognize MCMV infected cells and undergo a proliferative burst to enlarge the overall pool of effector cells, followed by a contraction of activated NK cells to form a long-lived population of memory NK cells[3]. To identify whether IRE1α promotes antiviral immunity of NK cells by regulating their adaptive traits, we co-transferred equal numbers of $Ly49H^+$ $IRE1^{NK}$ and CD45.1 congenic wild-type (WT) NK cells into Ly49H-deficient hosts and evaluated the ability of the transferred $Ly49H^+$ cells to expand following MCMV infection (Fig. 2c and Supplementary Fig. 3a). Whereas the transferred WT NK cells expanded robustly by day 7 PI, their $IRE1^{NK}$ counterparts were dramatically reduced (Fig. 2d,e). Moreover, the relative ratio of WT to $IRE1^{NK}$ cells remained elevated throughout the time course, ruling out a delayed expansion of the $IRE1^{NK}$ population (Fig. 2e).

Reduction of $IRE1^{NK}$ cells in peripheral blood was not due to selective aberrant trafficking, as similar deficiencies were found in spleen, liver, lung, BM and lymph nodes (Fig. 2f). A similar expansion defect was observed in NK cells lacking IRE1α's downstream substrate XBP1 (mice termed $XBP1^{NK}$, Fig. 2g, h and Supplementary Fig. 2b–d). Transcriptomics revealed no change in expression of well-defined IRE1-dependent decay of mRNA ('RIDD') target genes (Supplementary Fig. 4), indicating that IRE1α functions primarily via controlling its major substrate XBP1 rather than by RIDD. In contrast to the expansion defect, NK cell activation, cytokine production and cytotoxicity on a per cell basis was unaffected by deletion of IRE1α (Supplementary Fig. 3b, c). Levels of Akt-mTOR signaling were unchanged in $IRE1^{NK}$ cells consistent with the placement of IRE1α-XBP1 downstream of mTOR (Supplementary Fig. 3d). We conclude that there is an essential cell-intrinsic function for IRE1α-XBP1 to promote clonal expansion of NK cells during viral infection.

Control of NK cell proliferation but not survival by IRE1α-XBP1

To determine whether IRE1α-XBP1 controls proliferation or survival/apoptosis in activated NK cells, we co-transferred $Ly49H^+$ $IRE1^{NK}$ and CD45.1 congenic WT NK cells labeled with a cell proliferation tracing dye into MCMV-infected Ly49H-deficient recipients and confirmed that IRE1α deficiency markedly impaired MCMV-driven proliferation *in vivo* (Fig. 3a–c). Diminished proliferative capacity of $IRE1^{NK}$ $Ly49H^+$ cells was corroborated by their reduced ability to incorporate EdU (5-ethynyl-2'-deoxyuridine) (Fig. 3d). $IRE1^{NK}$ cells did not exhibit enhanced apoptosis, as determined by Annexin V or activated caspases staining (Fig. 3e, f). Hence IRE1α is required for the proliferation but not survival of activated NK cells during viral infection.

Because IRE1α activation is induced to a similar extent in both antigen-specific Ly49H^{+} and bystander Ly49H^{-} [26] NK cells during MCMV infection (Fig. 1c), it was possible that IRE1α could regulate cytokine-driven NK cell proliferation independently of Ly49H-m157 engagement. Indeed, even adoptively transferred Ly49H^{-} NK IRE1^{NK} cells showed impaired proliferation (Fig. 3c), albeit to a lesser extent than MCMV infected Ly49H^{+} NK cells.

IRE1α-XBP1 drives NK cell homeostatic proliferation

Robust NK cell expansion can also be triggered by lymphopenia (homeostatic proliferation)[27]. Co-transfer of equal numbers of IRE1^{NK} and CD45.1 congenic WT splenic NK cells into lymphocyte-deficient (recipient *Rag2*$^{-/-}$ *Il2rg*$^{-/-}$ mice) hosts (Fig. 4a) revealed that IRE1α deficiency leads to ~2.5 fold lower homeostatically-driven NK cells (Fig. 4b) due to decreased proliferation (Fig. 4c). Thus, although IRE1α-XBP1 may be dispensable for NK cell development and basal homeostasis at steady state (Supplementary Fig. 2b–f), IRE1^{NK} cells exhibit dramatically compromised homeostatic proliferation during lymphopenia.

IL-2 and IL-15, cytokines of the common gamma chain family, expand[28, 29] and induce XBP1 splicing in NK cells *ex vivo* from mouse spleen, BM and human PBMCs (Fig. 1e, f). A 1:1 co-culture of IRE1^{NK} and CD45.1 congenic WT NK cells with IL-2 and IL-15 revealed that IRE1^{NK} cells were continually outcompeted by WT cells (Fig. 4d). Interestingly, IRE1^{NK} cells did not ‘blast’ (a common characteristic of proliferating cells) as much as their WT counterparts (Fig. 4e). and proliferated less well than IRE1$^{f/f}$ littermate NK cells cultured with IL-2 and IL-15 (Fig. 4f, g) although they expressed normal levels of these cytokine receptors (Supplementary Fig. 2f), ruling out hyposensitivity to cytokine signaling as the reason for their reduced proliferation. Additionally, pharmaceutical blockade of IRE1α activity using 4μ8C[30] small molecule inhibitor of the IRE1α RNase domain – led to significant reduction in proliferation of primary human NK cells cultured in IL-2 and IL-15 (Fig. 4h, Supplementary Fig. 4b). Interestingly, 4μ8C primarily hindered the proliferation of CD56^{bright} NK cells (Fig. 4i), a subset of human NK cells with higher proliferative capacity compared to CD56^{dim} counterparts[29] and consistent with a more robust induction of XBP1s protein in CD56^{bright} NK cell subsets (Fig. 4j). Thus, IRE1α-XBP1’s function in growth and proliferation is conserved between mouse and human NK cells..

IRE1α-XBP1 promotes oxidative phosphorylation in NK cells

To identify key cellular processes and molecular mediators downstream of IRE1α-XBP1 in proliferating NK cells, we generated mixed IRE1^{NK} (CD45.2): WT (CD45.1) BM chimera mice[31] (Supplementary Fig. 2e) and performed whole genome transcriptome analysis on IRE1^{NK} and WT Ly49H^{+} NK cells harvested at day 0, 1.5, and 7 PI. IRE1^{NK} cells showed an overall transcriptome profile similar to their WT counterparts prior to infection, with 76 genes differentially expressed at day 0 (Fig. 5a). Importantly, the gene expression profile of

IRE1^{NK} cells at day 1.5 PI was markedly distinct from WT NK cells, with 897 genes differentially expressed (Fig. 5a).

Activated immune cells undergo robust metabolic responses, key for regulating immune cell function and long-term fitness[32]. Activation of NK cell oxidative phosphorylation (OXPHOS) and glycolysis is essential for robust NK cell responses[33, 34]. Interestingly, OXPHOS was highlighted as the top downregulated cellular process in IRE1^{NK} cells by GO analysis (Fig. 5b, c). Metabolic flux analysis on IL-12 and IL-18 activated human primary NK cells showed significantly decreased mRNA levels of OXPHOS signature and reduced maximal respiration rate upon blockade of IRE1α activity with 4μ8C (Fig. 5d). Consistent with this, electron microscopy revealed disrupted mitochondrial morphology on sorting-purified IRE1^{NK} cells during MCMV infection (Supplementary Fig. 5). Collectively, the molecular, cellular and metabolic evidence suggests a critical role of IRE1α-XBP1 in supporting OXPHOS in NK cells.

XBP1 promotes NK cell proliferation in part by direct transactivation of c-Myc expression

We used the QIAGEN Ingenuity Pathway Analysis platform to identify key molecular mediators of proliferation in IRE1^{NK} cells. Both XBP1 (top 1, $p = 2.66^{-38}$) and IRE1α (gene name Ern1, top6, $p = 6.23^{-8}$) were among the top upstream regulators in IRE1^{NK} cells providing validation (Supplementary Fig. 6a). Surprisingly, reduction of transcription factor Myc (N-Myc, top2, $p = 3.93^{-28}$; c-Myc, top 5, $p = 4.75^{-8}$) in IRE1^{NK} vs WT NK cells was predicted and the Myc signaling pathway was also identified by GO analysis (Fig. 6a) Further, we observed significantly reduced expression of Myc targets that control cell proliferation or processes highly related to cell growth in IRE1^{NK} cells (Fig. 6b). Although Myc controls a range of biological processes including cell growth, protein synthesis and cell metabolism[35, 36], its importance in NK cell responses is less well studied[33]. Interestingly, although there is significant overlap between IRE1α-regulated and Myc-regulated genes identified in MCMV-primed NK cells (Supplementary Fig. 6b), Myc has not previously been described as a target of IRE1α-XBP1.

We investigated the kinetics of Myc expression in differentiating NK cells, and its potential correlation with IRE1α-XBP1 activation. N-Myc was undetectable in NK cells at all time points following MCMV infection, whereas basal levels of *c-Myc* mRNA were observed in naïve NK cells (Supplemental Fig. 6c). No appreciable expression of c-Myc protein was evident at baseline (Supplemental Fig. 6c), attributed perhaps to c-Myc protein instability secondary to multiple degradation mechanisms[37]. Following MCMV infection, NK cells robustly upregulated *c-Myc* mRNA, and protein levels were now easily detectable (Supplemental Fig. 6c). Furthermore, in MCMV-infected ERAI mice, levels of c-Myc protein correlated with IRE1α activity (Supplemental Fig. 6c). These data suggest that engagement of both the IRE1α-XBP1 UPR and c-Myc are important during NK cell priming.

To test whether IRE1α-XBP1 is required for c-Myc induction, we measured c-Myc expression in IRE1^{NK} cells. The basal levels of *c-Myc* mRNA and protein were unaffected by the absence of IRE1α in naïve NK cells (Supplemental Fig. 6d). During MCMV infection, c-Myc transcript and protein levels were significantly diminished in IRE1^{NK} cells compared to WT counterparts (Fig. 6c–e). Furthermore, suboptimal upregulation of canonical c-Myc targeting genes was observed in IRE1^{NK} cells (Supplementary Fig. 6e). Consistent with the notion that c-Myc acts as a transcriptional repressor of the cell cycle checkpoint protein p21[38], mRNA levels of *Cdkn2a* were significantly upregulated by depletion of IRE1α (Supplemental Fig. 6e). Because c-Myc expression was not completely eradicated in the absence of IRE1α, complementary upstream mechanisms likely exist (i.e. mTOR, Supplementary Fig. 6h). nduction of the c-Myc protein during homeostatic proliferation was also impaired in IRE1^{NK} cells (Supplementary Fig. 6i). Together, these results indicate that IRE1α-XBP1 activation regulates c-Myc expression in NK cells.

XBP1s acts as a versatile transcription factor that facilitates adaptation to ER stress by regulating distinct sets of target genes involved in protein folding and quality control[9]. Putative XBP1-binding sites[39] were found in both human and mouse *c-Myc* promoter regions (Supplementary Fig. 6f). Chromatin immunoprecipitation assays performed on a mouse NK/ILC cell line (MNK-1) phenotypically and functionally similar to primary mouse NK cells[40], and on two human NK cell lines derived from patients with aggressive NK leukemia/lymphoma (NKL[41] and KHYG-1[42]) revealed a robust enrichment of XBP1 binding to the *c-Myc* promoter region (Fig. 6f),. We also utilized a c-Myc reporter mouse strain (referred to as 'Myc^{GFP}) to assess the extent to which *c-Myc* promoter activation is dependent on IRE1α. Myc^{GFP} NK cells were stimulated *in vitro* in the presence or absence of 4μ8C. Whereas c-Myc reporter GFP was induced upon treatment with either IL-15, or IL-12 and IL-18 in DMSO-treated control groups, GFP induction was largely impeded by IRE1α blockade (Fig. 6g). Our data demonstratet that IRE1α positively regulates c-Myc transcription in activated NK cells by direct binding of XBP1 to the *c-Myc* promoter.

To evaluate c-Myc function in the expansion of activated NK cells, we generated mice that harbor NK cells with haploinsufficiency in c-Myc (referred to as Myc^{NK}, Supplemental Fig. 7). If IRE1α-XBP1 regulates NK cell expansion primarily via its impact on c-Myc, we would predict that Myc^{NK} cells would show a similar defect to IRE1^{NK} cells. Indeed, when equal numbers of Myc^{NK} and CD45.1 congenic WT Ly49H^{+} NK cells were co-transferred into Ly49H-deficient recipients infected with MCMV, WT NK cells outcompeted Myc^{NK} cells during the entire course of the response (Fig. 5h). Thus, c-Myc deficiency impairs clonal expansion of NK cells in a manner similar to NK cells lacking IRE1α or XBP1.

To formally test the hypothesis that IRE1α-XBP1 functions at least in part by regulating c-Myc in activated NK cells to facilitate their proliferation, we generated mice that harbor NK cells with overexpression of c-Myc (Myc$^{fsf/+}$ Ncr1^{Cre+}, referred to as Myc^{OE}). Levels of *c-Myc* were moderately elevated by 2-fold in Myc^{OE} NK cells compared to littermate controls (Fig. 7a), although this conferred no appreciable advantage in proliferation during *in vitro* expansion (Fig. 7b–e). We posited that if c-Myc is a primary mediator of IRE1α-XBP1 activity, then overexpression of c-Myc should restore NK cell proliferation when IRE1α is pharmaceutically blocked or genetically depleted. Indeed, we found that during *in vitro* expansion, NK cells from WT littermates (Myc$^{fsf/+}$ Ncr1^{Cre-}) had impaired proliferation after treatment with 4μ8C; however, NK cells from Myc^{OE} mice were largely rescued from this defect and proliferated to a comparable extent as in the DMSO-treated control group (Fig. 7b). Thus, the requirement of IRE1α-XBP1 for NK cell proliferation can be partially bypassed by moderate overexpression of c-Myc. We further crossed Myc^{OE} with $IRE1^{NK}$ mice to overexpress c-Myc in NK cells with genetic deletion of IRE1α. The delayed proliferation observed in $IRE1^{NK}$ cells was significantly alleviated by restoration of c-Myc via genetic overexpression (Fig. 7c–e). Collectively, these findings reveal a novel XBP1-Myc axis that regulates NK cell expansion during infection and homeostatic proliferation.

Requirement for IRE1α/XBP1 in NK cell-mediated antitumor immunity

In addition to antiviral responses, NK cells play an essential role in the host antitumor response[43, 44, 45, 46]. The experimental intravenous B16 melanoma model provides a potent functional measurement of NK cell-mediated antitumor protection. Thus, we introduced B16F10 tumor cells intravenously to $IRE1^{NK}$ and $IRE1^{f/f}$ littermates. While the majority of $IRE1^{f/f}$ mice were protected from lung tumor colonization at day 10 after inoculation, $IRE1^{NK}$ mice exhibited significantly more melanoma nodules (Fig. 8a) and micro-metastatic lesions (Fig. 8b). Survival of melanoma-bearing $IRE1^{NK}$ mice was significantly decreased and inversely correlated with the increased tumor burden (Fig. 8c). Similar to $IRE1^{NK}$ mice, $XBP1^{NK}$ mice also failed to control melanoma growth (Fig. 8d), consistent with a role for XBP1 downstream of IRE1α in NK cells. Similar to the defect in expansion in $IRE1^{NK}$ cells during viral infection, the lungs from tumor-inoculated $IRE1^{NK}$ mice displayed a 50–70% reduction in percentages and absolute numbers of infiltrating NK cells compared to $IRE1^{f/f}$ littermates lungs (Fig. 8e), and significantly decreased levels of proliferation marker Ki-67 (Fig. 8f) and transcription factor c-Myc (Fig. 8g). Of note, the decreased number of NK cells and decreased levels of Ki-67 and c-Myc (Fig. 8e–g) were only apparent following tumor injection, as no changes were detected in tumor-free animals (Supplementary Figs. 8a, and 2b). These findings demonstrate that the IRE1α-XBP1 pathway is required for optimal NK cell expansion that facilitate host protection against NK cell-sensitive cancer.

Discussion

We demonstrate that the IRE1α-XBP1 branch of the ER Stress Response is a previously unrecognized key signaling pathway in NK cells essential for their function in viral infection, homeostatic proliferation and cancer. NK cells lacking either the upstream sensor IRE1α or its downstream substrate XBP1 fail to expand in response to MCMV infection, lymphopenia or melanoma. Mechanistically, IRE1α-XBP1 directly regulate c-Myc signaling and mitochondrial respiration to control NK cell proliferation. Hence the mammalian immune system has evolved a mechanism to incorporate a common cellular stress process to enhance antiviral immunity. The fact that this conserved pathway is co-opted by pathogens to ensure their survival in host cells[47] provides intriguing evidence for host-virus coevolution.

The host immune system controls viral infection primarily through early activation of innate NK cells followed by adaptive responses by $CD8^+$ cytotoxic T cells. NK cells recognize infected cells without prior sensitization to counteract infection by initiating effector functions including cytotoxicity, cytokine production, and proliferation[7]. However, less is known about the intrinsic regulators that control their function or expansion[5, 6]. Here we identify the ER Stress Response as an essential driver of NK cell expansion *in vivo* during

MCMV infection. CMV is a leading cause of birth defects in newborns and a dangerous pathogen in immunocompromised individuals (including cancer and transplant patients). No effective vaccine against CMV is available[48]. We demonstrate that human primary NK cells activate IRE1α-XBP1 in response to pro-inflammatory cytokines present during CMV infection and rely on this pathway for optimal *ex vivo* expansion. IRE1α activation may help develop new vaccine strategies for host control of pathogens by strengthening NK cell responses.

In patients and animal models, impaired NK cell function is associated not only with recurring viral infection, but also with an increased incidence of various malignancies[7, 49, 50]. NK cells whose "primed" cytotoxicity is elicited by activating receptor signaling[51, 52], and their ability to recruit other immune cells into the tumor microenvironment[46] play a pivotal role in cancer immunosurveillance. The failure to control melanoma lung metastasis is associated with impaired expansion of the NK cell compartment, providing the first *in vivo* indication that IRE1α-driven NK cell expansion is critical for tumor immunosurveillance. The deficiency in NK cell expansion correlates with reduced recruitment of type 1 conventional dendritic cells and $CD8^+$ T cells consistent with the notion that NK cells not only function as direct killers but also potentiate an antitumor microenvironment[46]. Future studies should investigate whether IRE1α-XBP1 represents the major signaling pathway that drives NK cell expansion in additional malignancies and to assess whether and to what extent other known regulators of NK cell expansion such as Zbtb32[5], Runx1/3[6] and IRF8[53] also contribute to halting tumor growth.

NK cells have recently attracted attention for their potential use as immune-based therapies[51, 52, 54, 55, 56], best documented in the setting of hematopoietic cell transplantation (HCT) in patients with leukemia[43]. Alloantigen-specific NK cells can benefit such patients by providing graft-versus-tumor function while preventing T cell-mediated graft-versus-host disease[44]. Leukemia patients undergoing immunoablative treatments before HCT often become susceptible to CMV[48], highlighting the key role of NK cells in eliminating both tumor and virus. In addition, NK cells are the first lymphocytes to reconstitute the BM of patients following HCT[43]. However, the magnitude of and mechanism underlying NK cell homeostatic proliferation in the setting of lymphopenia are poorly understood[3, 27, 57]. We demonstrate that -although unnecessary for normal NK cell expansion during development - IRE1α-XBP1 is indispensable for the homeostatic proliferation of mature NK cells *in vivo* in response to lymphopenia-induced stress, and for IL-15-driven homeostatic-like proliferation of human primary NK cells largely provided by the $CD56^{bright}$ highly proliferative subset. Our findings provide justification for incorporating NK cells into adoptive cellular immunotherapies to target cancer in patients following immunoablative treatment[7, 50], and suggest that pre-treatment of NK cells with a combination of cytokines (for instance, IL-15, IL-12 and IL-18 that are now being used in the clinic) might further increase the therapeutic efficiency of adoptive NK cell transfer. As this paper was being revised after peer review, it was reported that XBP1 is important *in vitro* for IL-15-driven human NK cell function[58]. By using newly-engineered genetic mouse models, our study demenstrates an essential *in vivo* requirement of the IRE1α-XBP1 pathway in NK cell-mediated antitumor and antiviral protection, and identifies novel cellular and molecular mechanisms of action not previously reported. Future studies should test the feasibility and efficacy of utilizing genetically manipulated IRE1α-XBP1-overexpressing "adaptive" NK cells to treat a variety of liquid or solid malignancies.

In sharp contrast to its protective role in activating NK cell immunity against CMV and melanoma described herein, overactive IRE1α-XBP1 in dendritic cells[17] and $CD4^+$ T cells[16] can cripple antitumor immune responses against ovarian cancer. The highly pleiotrophic functions of this pathway and the unique molecular mechanisms that govern those functions in different organs and cell types may explain the disparate effects of overactivation or silencing of this UPR branch. For example, the upstream pathways of IRE1-XBP1 vary among cell types. In macrophages, activation is induced through Toll-like receptor signaling while in NK cells, as shown here, both IL-12-STAT4 and mTOR act as critical upstream regulators of IRE1α-XBP1 under infectious/inflammatory conditions. Indeed mTOR is also situated downstream of IL-15[28, 59] and IL-12[33] and is essential for NK cell development and antitumor responses[60]. A recent publication demonstrated that mTOR drives IRE1α-XBP1 activation in liver in response to food perception[22], as well as in lung T_H2 cells and fibroblasts in fibrotic disease[23, 24].

We also report the unexpected finding that XBP1 directly controls the transcription of *c-Myc* and its downstream target genes in NK cells. This may appear paradoxical in light of the recent finding that the oncogene *c-Myc* acts upstream of the IRE1α-XBP1 pathway to drive tumorigenesis[61]. However, this discrepancy may be explained by the differing functions and downstream consequences of IRE1α signaling in normal versus transformed cells. One clear difference between transformed versus normal cells is that the former are addicted to constitutively activated c-Myc while the latter display negligible levels of c-Myc at baseline, requiring external stimuli to be induced. Although *c-Myc* is among the best-studied oncogenes and tumor-intrinsic c-Myc activity can program an immune suppressive microenvironment obligatory for tumor progression[62], its function in immune cells is less understood[63]. c-Myc is essential for metabolic responses in IL-2 and IL-12-activated mouse NK cells *ex vivo*[33]. In human NK cells *ex vivo*, c-MYC functions downstream of IL-15 to enhance effector function[64]. Here, we provide the first *in vivo* evidence of an essential role for c-Myc acting downstream of IRE1α-XBP1 to drive NK cell expansion during MCMV infection, lymphopenia and antitumor immunity. Indeed c-MYC levels were noted to be significantly decreased in NK cells from cancer patients compared to healthy donors[65], suggesting a protective role of c-MYC in NK cell-mediated antitumor immunity in patients.

Finally, our finding that IRE1α supports mitochondrial function and morphology in NK cells was unexpected given that we have recently described that depletion of IRE1α-XBP1 helps to restore the metabolic fitness of T cells in ovarian cancer[16]. Intriguingly, 25 of the 46 differentially expressed OXPHOS genes in IRE1α-deficient NK cells are known to be regulated by c-Myc[35]. Thus, the dysregulated metabolism observed here may be in part a consequence of impaired Myc signaling[33] which is in turn at least partly responsible for the failure of IRE1α-deficient NK cells to expand appropriately *in vivo* in response to viral infection, lymphopenia and malignancy.

In conclusion, our study reveals a novel and essential function for the ER stress sensor IRE1α and its downstream substrate XBP1 to drive NK cell expansion that results in effective responses against viral infection and tumors. IRE1α activation is situated downstream of both the Stat4 and mTOR signaling pathways and upstream of c-Myc. Like c-Myc, IRE1α-XBP1 also promotes OXPHOS in NK cells. We have identified a novel IRE1α-XBP1-cMyc axis in NK cell immunity, required for host protection against infection and cancer.

Methods

Mice

Mice were bred at Dana-Farber Cancer Institute in accordance with the guidelines of the Institutional Animal Care and Use Committee (IACUC). The following strains were used in this study, all on the C57BL/6 genetic background: C57BL6/J ($CD45.2^+$; The Jackson Laboratory), B6.SJL ($CD45.1^+$; The Jackson Laboratory), $Rag2^{-/-}Il2rg^{-/-}$(Taconic), Klra8−/− (Ly49H-deficient)[66], $IRE1^{f/f}$[67], $XBP1^{f/f}$[11], $Myc^{f/f}$ (a generous gift from Dr. Ruoning Wang), $Ncr1^{iCre}$ (a generous gift from Dr. Eric Vivier), ERAI (ER stress-activated indicator)[19], and GFP-c-Myc KI (here called Myc^{GFP}, the Jackson Laboratory). $Myc^{fsf/fsf}$ on mixed B6.126 background was a generous gift from Dr. Rosaline Sears. $IRE1^{f/f}$ $Ncr1^{iCre/WT}$ (here called $IRE1^{NK}$), $XBP1^{f/f}$ $Ncr1^{iCre/WT}$ ($XBP1^{NK}$), $Myc^{f/+}$ $Ncr1^{iCre/WT}$ (Myc^{NK}), $Myc^{fsf/+}$ $Ncr1^{iCre/WT}$ (Myc^{OE}) and $Myc^{fsf/+}$ $IRE1^{f/f}$ $Ncr1^{iCre/WT}$ (Myc^{OE} $IRE1^{NK}$) animals and littermate controls were generated by breeding at Dana-Farber Cancer Institute. Recipient Klra8−/− ($CD45.1^+CD45.2^+$) mice were generated by crossing Klra8−/− ($CD45.2^+$) to B6.SJL ($CD45.1^+$). Experiments were conducted using age- and gender-matched mice in accordance with approved institutional protocols.

Virus infection

MCMV (Smith strain) was passaged serially through BALB/c hosts two times, then viral stocks were prepared by using a dounce homogenizer to dissociate the salivary glands of infected mice 3 weeks after infection. For direct infection of C57BL/6 or ERAI mice, 7.5×10^3 plaque-forming units (PFU) of MCMV was injected by i.p.. For the adoptive transfer studies, Ly49-deficient mice were infected by i.p. injection of 7.5×10^2 PFU of MCMV one day after receiving approximately 2×10^5 $Ly49H^+$ NK cells by intravenous (i.v.) injection.

NK cell enrichment and adoptive transfer

Enrichment of NK cells was performed using the magnetic bead-based negative selection kit (Miltenyi Biotec) per the manufacturer’s protocol (typically 50–70% purify) before the flow cytometric analysis of the transferred NK cells in the spleen of recipients at early time points after infection of MCMV in some experiments (Fig. 3c–f, Fig. 6e). As previously described[31], for experiments involving co-transfer of $CD45.1^+$ and $CD45.2^+$ populations, equal numbers of $Ly49H^+$ NK cells (normalized on $KLRG1^{Lo}$ population) from each population were co-transferred together by intravenous injection into the tail vein of adult Ly49H-deficient recipients 1 d before infection with MCMV, or equal numbers of NK cells from each population were co-transferred together into adult $Rag2^{-/-}$x$Il2g^{-/-}$ recipients. WT and KO NK cells are transferred together into the same mouse and the numbers of cells are the same. Thus, the percentages shown are directly correlated with the absolute number of cells. In some experiments, cells were labeled before transfer with CellTrace Violet (CTV; Invitrogen) to trace cell proliferation.

Flow cytometry and cell sorting

Cell surface staining of single-cell suspensions was performed using the following fluorophore-conjugated antibodies (purchased from BD Biosciences, eBioscience, BioLegend, Tonbo Biosciences, Cell Signaling Technology, and R&D Systems): NK1.1 (PK136), KLRG1 (2F1), Ly49H (3D10), CD45.1 (A20), CD45.2 (104), CD8α (53–6.7), TCRβ (H57–597), CD3ε (145–2C11), F4/80 (BM8), CD19 (eBio1D3), Ki-67 (SolA15), c-Myc (D84C12), and XBP1s (Q3–695). Unless otherwise indicated, NK cells were defined as $CD19^{-}CD3^{-}$ $TCR\beta^{-}$ $F4/80^{-}$ $NK1.1^{+}$ cells. All analysis was performed on viable populations by exclusion of the dead cells using a fixable viability dye (Thermo Fisher). For the evaluation of NK cell apoptosis, Pan-caspase (FLICA) staining was carried out using the FAM FLICA *in vitro* Poly Caspase Kit (Immunochemistry Technologies) per the manufacturer’s protocol; Annexin V staining was carried out using the Invitrogen eBioscience Annexin V Apoptosis Detection Kit per the manufacturer’s instructions. For the evaluation of NK cell proliferation, cells were labeled with 5 uM CTV (Invitrogen) according to the manufacturer’s protocol before transfer into recipient mice; intracellular staining of Ki-67, c-Myc and XBP1s was performed by fixing and permeabilizing with the Foxp3/Transcription Factor Staining Kit (eBioscience); for the EdU labeling experiments, mice were subjected to i.p. injection of 1.5 mg of EdU in PBS on days 3.5 after infection with MCMV, and EdU labeling was determined ~16 h later using the Click-iT EdU Assay Kit (Thermo Fisher Scientific). Flow cytometry was performed on the LSR II (BD Biosciences), LSR Fortessa X-20 and CytoFLEX LX (Beckman Coulter). Cell sorting was performed on Aria II cytometers (BD Biosciences). For experiments involving qRT-PCR, cell populations were sorted to >95% purity. Data were analyzed with FlowJo software (Tree Star).

Ex vivo stimulation of primary mouse and human NK cells

For Fig. 1e, ~2×10^5 NK cells were stimulated for 16 hr in complete RPMI containing 10% FBS with recombinant mouse IL-2 (10 μg/ml; BioLegend), either in the presence or absence of IL-12 (20 ng/ml; Peprotech) and IL-18 (10 ng/ml; R&D Systems), or IL-15/15R (100 ng/ml, eBioscience. For *ex vivo* NK cell expansion experiments, 1.5×10^5 to 2.5×10^5 purified NK cells were stimulated in RPMI supplemented with 10% FBS, penicillin-streptomycin, L-glutamine and β-mercaptoethanol, and with recombinant mouse IL-2 (10 ng/ml; R&D Systems) and IL-15/15R (40 ng/ml; eBioscience) re-applied every other day. In some assays indicated, 5 uM of 4μ8C (IRE1α inhibitor; Sigma Aldrich) was added to the culture and DMSO was used as the control treatment.

Peripheral blood mononuclear cells (PBMCs) from healthy donors (New York Blood Center) were isolated by density gradient centrifugation with Ficoll (GE Healthcare). NK cells were enriched by negative selection using the human NK Cell Isolation Kit (Miltenyi Biotec; >90% purity). For *ex vivo* stimulation in Fig. 1f, ~10^6 sorted primary human NK cells were stimulated for 16 hr in complete RPMI containing 10% FBS with recombinant human IL-2 (10 μg/ml; Sigma Aldrich), in combination with either IL-12 (20 ng/ml;

StemCell) and IL-18 (10 ng/ml; Thermo Figher Scientific), or IL-15 (40 ng/ml, StemCell). For human NK *ex vivo* expansion in Fig. 4h, i, recombinant human IL-2 (100U/ml, Roche) and IL-15 (10 ng/ml, StemCell) was applied. Fresh medium and cytokines were added on alternating days of culture. In some assays indicated, 4μ8C (IRE1α inhibitor, 5 μM or lower) was added to the culture and DMSO was used as the control treatment. For flow cytometric analysis or cell sorting, human NK cells were defined as $CD3^{-}$ $CD56^{+}$.

NK cell lines and culture conditions

MNK-1 cells[40] were cultured in DMEM supplemented with 10% FBS, 2 mM GlutaMAX, 1 mM sodium pyruvate, 55 μM 2-mercaptoethanol, 10 mM HEPES, 50 μg/ml gentamicin, 100 U/ml penicillin, and 100 μg/ml streptomycin (all from Corning or Gibco Life Technologies, except FBS from Atlanta Biologicals). To facilitate robust survival, 10 ng/ml recombinant mouse IL-2 (BioLegend) were re-applied daily. NKL cells[41] and KHYG-1 cells[42] were cultured in RPMI 1640 medium supplemented with 2 mM L-glutamine, 1 mM sodium pyruvate, 100 U/ml penicillin, 100 μg/ml streptomycin and 7.5% FCS plus 7.5% new born calf serum (all from Corning or Gibco Life Technologies, except FBS from Atlanta Biologicals). The cell concentration was maintained at ~5×10^{5} /ml in the presence of 50 U/ml of recombinant human IL-2 (Amgen). All cell lines routinely tested negative for mycoplasma contamination using the Mycoplasma Detection Kit (Lonza) and maintained in medium containing plasmocin (Invivogen) for prophylactic purpose.

Quantitative real time PCR

Cells were pre-enriched (Miltenyi Biotec) and then sorted to >95% purity and RNA was isolated using the RNeasy RNA purification mini (for 5×10^{5} cells or beyond) or micro (for $<5 \times 10^{5}$ cells) kit (Qiagen) according to the manufacturer's protocol. From purified RNA, cDNA was synthesized using the reverse-transcriptase kit qScript cDNA synthesis kit (Quanta Biosciences). Quantitative real time PCR (qRT-PCR) was performed in triplicates in a 384-well plate using Taqman Probes (Themo Fisher) or SYBR Green (Quanta Biosciences) -based detection on an ABI QuantStudio 6 Flex qRT-PCR machine. For experiments in Fig. 6c, CellDirect One-Step qRT-PCR Kit with Rox (Life Technologies) was used according to the manufacturer's instruction. For the analysis of mRNA abundance, the derived values were normalized to those of β-Actin (β-ACTIN for human materials). Primer sequences are in Supplementary Table 1 and Taqman probe information is in Supplementary Table 2.

RNA-seq analysis

Mixed $IRE1^{NK}$ (CD45.2): WT (CD45.1) BM chimeric mice were generated as previously described[31]. Briefly, host C57BL/6 × B6.SJL animals ($CD45.1^{+}CD45.2^{+}$) were lethally irradiated with 900 grays of radiation and reconstituted with a 1:1 mixture of BM cells from B6.SJL WT ($CD45.1^{+}$) and knockout or transgenic donor ($CD45.2^{+}$) mice, co-injected with anti-NK1.1 (clone PK136) to deplete any residual donor or host mature NK cells. $CD45.1^{+}CD45.2^{+}$ host NK cells were excluded from all analyses.

Mice were infected with 7.5×10^{3} PFU of MCMV by i.p. injection and spleens were harvested at day 0, 1.5 and 7 after infection. Total RNA from sorting-purified $Ly49H^{+}$ WT or IRE1^{NK} NK cells was extracted with the RNeasy RNA purification micro kit (Qiagen) according to the manufacturer's instructions. Poly(A)+ RNA-seq libraries (pair-end 100) were prepared with an Illumina TruSeq RNA Sample Preparation Kit V2 according to the manufacturer's instructions (Illumina). Sequence data from Illumina's HiSeq4000 sequencer were 'de-multiplexed' to generate FASTQ files for each sample with Illumina's CASAVA pipeline (version 1.8.2).

The reads that passed Illumina's quality and purity filter (> 90%) were aligned to the mouse genome (Illumina iGenomes mm9 build) with tophat2[68] with default parameters. The resulting SAM alignment files were then converted to the BAM file format, then were sorted and indexed with SAMtools (version 0.1.14). The HTSeq[69] was used for summarization of the aligned sequence reads into counts. Differential gene expression was analyzed with the DESeq2[70]. Transcripts with adjusted P value < 0.01 were considered differentially expressed between genotypes (wild-type and IRE1^{NK}) and infection times (day 0, 1.5, 7). Gene ontology analysis of differentially expressed genes was performed in GSEA (gene sets enrichment analysis)[71]. Pathway analysis of predicted upstream regulators was performed with Ingenuity Pathway Analysis software (Qiagen). For heat maps, normalized data from DESeq RNA-seq analyses were exported, manually curated for specific genes in each category, and the gene-expression z-score was visualized with the Heatmap.2 function within the gplots R library.

Chromatin immunoprecipitation (CHIP)

MNK-1, NKL and KHYG-1 cells were crosslinked with 1% formaldehyde for 10 min at room temperature. Reaction was quenched with 125mM glycine. CHIP was performed as previously described[72] with XBP1 antibody (Cat. 619502, Biolegend), or normal rabbit IgG control (Cat. #2729, CST). The sequences of all primers are listed in Supplementary Table 3.

Immunoblots

Sorted purified NK cells (purity>97%) from WT: IRE1^{NK} mixed BM chimeras day 1.5 PI were collected directly into 20% TCA (trichloroacetic acid) buffer. After sorting, the concentration of TCA was adjusted to 10% before incubation on ice for 30 min to precipitate proteins. The homogenates were centrifuged at 13, 000 r.p.m. for 10 min at 4°C, and the supernatant was carefully removed. The pellets with concentrated proteins were washed twice with acetone, and then solubilized in solubilization buffer (containing 9M Urea, 2% Triton X-100, and 1% DTT) mixed with LDS buffer (Invitrogen). The samples were heated at 70°C for 10min and protein concentrations determined using a BCA protein assay kit (Thermo Fisher Scientific). Equivalent amounts of protein for WT and KO cells from the same BM chimeras were separated by SDS–PAGE (Bis-Tris gel, Invitrogen) and transferred onto PVDF membranes following the standard protocol. Anti-cMyc (D84C12, Cell Signaling Technology), anti-β-Actin (Cell Signaling Technology) and goat anti-rabbit secondary antibodies conjugated wiih HRP (Thermo Fisher Scientific) were used. SuperSignal West Pico and Femto chemiluminescent substrates (Thermo Fisher Scientific) were used to image blots in a ChemiDoc™ MP Imaging System instrument (BioRad). Densitometric quantification was performed using Image J software (NIH).

Metabolic flux assays

Purified human primary NK cells from healthy PBMC donors were stimulated with human recombinant IL-12 and IL-18 for 16hr in complete RPMI medium, in the presence or absence of IRE1 inhibitor 4μ8C (5 μM). After incubation, NK cells were collected, thoroughly washed and then subjected to Seahorse analyses using non-buffered XF base medium containing 25 mM glucose, 2 mM L-glutamine, and 1 mM sodium Pyruvate but lacking serum. XF96 cell-culture microplates were coated with CellTak (Corning) before analysis according to the manufacturer's instructions and washed twice with distilled water. 6×10^5 NK cells were plated and OCR measurements were analyzed on an XFe96 Extracellular Flux Analyzer (Agilent). After Basal OCR measurements were obtained, an OCR trace was recorded in response to oligomycin (1 μM), carbonyl cyanide-p-(trifluoromethoxy) phenylhydrazone (FCCP, 1 μM), and rotenone and antimycin (0.5 μM each) following the XF Cell Mito Stress test kit (Agilent). Metabolic parameters were calculated as follows: basal OCR = last rate measurement before oligomycin injection – minimum rate measurement after rotenone and antimycin injection; maximal OCR = maximum rate measurement after FCCP injection – minimum rate measurement after rotenone and antimycin injection. Typically, 3–6 technical replicates per each sample were examined. OCR values were normalized by protein input amount accordingly.

Experimental melanoma lung metastasis

B16F10 cells[73] were cultured in DMEM supplemented with 10% FBS, 100 U/ml penicillin and 100 ug/ml streptomycin. 2.0×10^5 B16F10 cells were injected intravenously through the tail vein. Mice were sacrificed and lungs were harvested on day 10–20 post inoculation. Lung tumor nodules were enumerated by gross count of visible sites of disease. Micrometastatic lesions were identified using H&E stained lung sections. All pulmonary tumor measurements were performed in a blinded manner. For the flow cytometric analysis, mice received an intravenous injection of fluorescence-conjugated anti-CD45.2 three minutes prior to euthanasia to label intravascular immune cells that would be excluded from downstream analysis. Lungs were harvested from tumor-bearing mice following euthanasia by CO_2 inhalation, and single-cell suspensions were obtained using a gentleMACS dissociator (Miltenyi Biotec) per manufacturer's instructions.

Statistics

For graphs, data are shown as mean ± s.e.m. or s. d. as indicated. and, unless otherwise indicated, statistical differences were evaluated using a two-tailed unpaired Student's *t*-test, assuming equal sample variance. $P < 0.05$ was considered significant. Graphs were produced and statistical analyses were performed using GraphPad Prism or R. Sample size was not specifically predetermined, but the number of mice used was consistent with prior experience with similar experiments.

Reporting Summary

Further information on research design is available in the Nature Research Reporting Summary linked to this article.

Data availability

The RNA-seq data were deposited in the Gene Expression Omnibus under the accession number GSE 113214. The remaining data that support the findings of this study are available from the corresponding authors upon request. Materials will be provided with material transfer agreements in place as appropriate.

Supplementary Material

Refer to Web version on PubMed Central for supplementary material.

Acknowledgements

We thank E. Vivier (Aix Marseille University) for NCR1^{iCre} mice; R. Wang (Nationwide Children's Hospital) for Myc$^{fl/fl}$ mice; R. Sears (Oregon Health & Science University) for Myc$^{fsf/fsf}$ mice; J. Ritz (Dana-Farber Cancer Institute) for the NKL cell line; C. Hurley (Georgetown University) for the KHYG-1 cell line; D. Lyden (Weill Cornell Medicine) for the B16F10 cell line; members of the Sun lab for sharing viral reagents, cytokines and flow cytometry antibodies, and for providing experimental assistance; members of the Glimcher lab – M. Raundhal, C. Lentucci, R. Xu, S. Shrestha and A. Gonzalez for technical support; S. Adoro (Case Western Reserve University) and J. Cubillos-Ruiz for critical reading of the manuscript and helpful discussion; M. Song (Weill Cornell Medicine) and the Wucherpfennig lab (Dana-Farber Cancer Institute) for insightful comments; J. Xiang (Weill Cornell Genomics and Epigenomics Core) for RNA-seq; J. McCormick (Weill Cornell Medicine) and DFCI Flow Cytometry Core for cell sorting; Specialized Histopathology Core at Brigham & Women's Hospital for histology; L. Cohen-Gould and J. Jimenez (Microscopy and Image Analysis Core Facility at Weill Cornell Medicine) for electron microscopy; X. Liu (Metabolism and Mitochondrial Research Core, Beth Israel Deaconess Medical Center) for metabolic flux assays; D. Neuberg (Dana-Farber Cancer Institute) for advising on statistical analysis; S. Schneider (Dana-Farber Cancer Institute) for manuscript editing. L.H.G. and H.D. were supported by Institutional Funding from The Dana-Farber Cancer Institute. H.D. was also supported by a Helen Gurley Brown Presidential Initiative Award (Dana-Farber Cancer Institute). J.C.S. was supported by the Ludwig Center for Cancer Immunotherapy, the American Cancer Society, the Burroughs Wellcome Fund, and the NIH (AI100874, AI130043, and P30CA008748). N.M.A.was supported by an MSTP Grant from the NIGMS of the NIH to the Weill Cornell/ Rockefeller/Sloan Kettering Tri-Institutional MD-PhD Program (T32GM007739), and by an F30 Predoctoral Fellowship from NIAID of the NIH (F30 AI136239). X. C. was supported by a NIH 1 R37 CA228304–01 grant.

References (for main text only)

1. Caligiuri MA Human natural killer cells. Blood 112, 461–469 (2008). [PubMed: 18650461]
2. Madera S et al. Type I IFN promotes NK cell expansion during viral infection by protecting NK cells against fratricide. J Exp Med 213, 225–233 (2016). [PubMed: 26755706]
3. Zawislak CL et al. Stage-specific regulation of natural killer cell homeostasis and response against viral infection by microRNA-155. Proceedings of the National Academy of Sciences of the United States of America 110, 6967–6972 (2013). [PubMed: 23572582]
4. Sun JC et al. Proinflammatory cytokine signaling required for the generation of natural killer cell memory. J Exp Med 209, 947–954 (2012). [PubMed: 22493516]
5. Beaulieu AM, Zawislak CL, Nakayama T & Sun JC The transcription factor Zbtb32 controls the proliferative burst of virus-specific natural killer cells responding to infection. Nature immunology 15, 546–553 (2014). [PubMed: 24747678]
6. Rapp M et al. Core-binding factor beta and Runx transcription factors promote adaptive natural killer cell responses. Sci Immunol 2 (2017).
7. Morvan MG & Lanier LL NK cells and cancer: you can teach innate cells new tricks. Nat Rev Cancer 16, 7–19 (2016). [PubMed: 26694935]
8. Yoshida H, Matsui T, Yamamoto A, Okada T & Mori K XBP1 mRNA is induced by ATF6 and spliced by IRE1 in response to ER stress to produce a highly active transcription factor. Cell 107, 881–891 (2001). [PubMed: 11779464]
9. Lee AH, Iwakoshi NN & Glimcher LH XBP-1 regulates a subset of endoplasmic reticulum resident chaperone genes in the unfolded protein response. Mol Cell Biol 23, 7448–7459 (2003). [PubMed: 14559994]

10. Lee AH, Heidtman K, Hotamisligil GS & Glimcher LH Dual and opposing roles of the unfolded protein response regulated by IRE1alpha and XBP1 in proinsulin processing and insulin secretion. Proceedings of the National Academy of Sciences of the United States of America 108, 8885–8890 (2011). [PubMed: 21555585]
11. Lee AH, Scapa EF, Cohen DE & Glimcher LH Regulation of hepatic lipogenesis by the transcription factor XBP1. Science 320, 1492–1496 (2008). [PubMed: 18556558]
12. Kaser A et al. XBP1 links ER stress to intestinal inflammation and confers genetic risk for human inflammatory bowel disease. Cell 134, 743–756 (2008). [PubMed: 18775308]
13. Chen X et al. XBP1 promotes triple-negative breast cancer by controlling the HIF1alpha pathway. Nature 508, 103–107 (2014). [PubMed: 24670641]
14. Condamine T et al. ER stress regulates myeloid-derived suppressor cell fate through TRAIL-R-mediated apoptosis. The Journal of clinical investigation 124, 2626–2639 (2014). [PubMed: 24789911]
15. Yan D, Wang HW, Bowman RL & Joyce JA STAT3 and STAT6 Signaling Pathways Synergize to Promote Cathepsin Secretion from Macrophages via IRE1alpha Activation. Cell reports 16, 2914–2927 (2016). [PubMed: 27626662]
16. Song M et al. IRE1alpha-XBP1 controls T cell function in ovarian cancer by regulating mitochondrial activity. Nature 562, 423–428 (2018). [PubMed: 30305738]
17. Cubillos-Ruiz JR et al. ER Stress Sensor XBP1 Controls Anti-tumor Immunity by Disrupting Dendritic Cell Homeostasis. Cell 161, 1527–1538 (2015). [PubMed: 26073941]
18. Beaulieu AM & Sun JC Tracking Effector and Memory NK Cells During MCMV Infection. Methods Mol Biol 1441, 1–12 (2016). [PubMed: 27177652]
19. Iwawaki T, Akai R, Kohno K & Miura M A transgenic mouse model for monitoring endoplasmic reticulum stress. Nat Med 10, 98–102 (2004). [PubMed: 14702639]
20. Madera S & Sun JC Cutting edge: stage-specific requirement of IL-18 for antiviral NK cell expansion. Journal of immunology (Baltimore, Md. : 1950) 194, 1408–1412 (2015).
21. Orr MT et al. Ly49H signaling through DAP10 is essential for optimal natural killer cell responses to mouse cytomegalovirus infection. J Exp Med 206, 807–817 (2009). [PubMed: 19332875]
22. Brandt C et al. Food Perception Primes Hepatic ER Homeostasis via Melanocortin-Dependent Control of mTOR Activation. Cell 175, 1321–1335 e1320 (2018). [PubMed: 30445039]
23. Hsu HS et al. Involvement of ER stress, PI3K/AKT activation, and lung fibroblast proliferation in bleomycin-induced pulmonary fibrosis. Sci Rep 7, 14272 (2017). [PubMed: 29079731]
24. Zheng H et al. Leptin Promotes Allergic Airway Inflammation through Targeting the Unfolded Protein Response Pathway. Sci Rep 8, 8905 (2018). [PubMed: 29891850]
25. Cerwenka A & Lanier LL Natural killer cell memory in infection, inflammation and cancer. Nat Rev Immunol 16, 112–123 (2016). [PubMed: 26806484]
26. Dokun AO et al. Specific and nonspecific NK cell activation during virus infection. Nature immunology 2, 951–956 (2001). [PubMed: 11550009]
27. Sun JC, Beilke JN, Bezman NA & Lanier LL Homeostatic proliferation generates long-lived natural killer cells that respond against viral infection. J Exp Med 208, 357–368 (2011). [PubMed: 21262959]
28. Mao Y et al. IL-15 activates mTOR and primes stress-activated gene expression leading to prolonged antitumor capacity of NK cells. Blood 128, 1475–1489 (2016). [PubMed: 27465917]
29. Wagner JA et al. CD56bright NK cells exhibit potent antitumor responses following IL-15 priming. The Journal of clinical investigation 127, 4042–4058 (2017). [PubMed: 28972539]
30. Cross BC et al. The molecular basis for selective inhibition of unconventional mRNA splicing by an IRE1-binding small molecule. Proceedings of the National Academy of Sciences of the United States of America 109, E869–878 (2012). [PubMed: 22315414]
31. Sun JC, Beilke JN & Lanier LL Adaptive immune features of natural killer cells. Nature 457, 557–561 (2009). [PubMed: 19136945]
32. Buck MD, Sowell RT, Kaech SM & Pearce EL Metabolic Instruction of Immunity. Cell 169, 570–586 (2017). [PubMed: 28475890]

33. Loftus RM et al. Amino acid-dependent cMyc expression is essential for NK cell metabolic and functional responses in mice. Nature communications 9, 2341 (2018).
34. O'Sullivan TE & Sun JC Innate Lymphoid Cell Immunometabolism. J Mol Biol 429, 3577–3586 (2017). [PubMed: 28867535]
35. Morrish F & Hockenbery D MYC and mitochondrial biogenesis. Cold Spring Harb Perspect Med 4 (2014).
36. van Riggelen J, Yetil A & Felsher DW MYC as a regulator of ribosome biogenesis and protein synthesis. Nat Rev Cancer 10, 301–309 (2010). [PubMed: 20332779]
37. Farrell AS & Sears RC MYC degradation. Cold Spring Harb Perspect Med 4 (2014).
38. Lu Y et al. MYC Targeted Long Noncoding RNA DANCR Promotes Cancer in Part by Reducing p21 Levels. Cancer Res 78, 64–74 (2018). [PubMed: 29180471]
39. Clauss IM, Chu M, Zhao JL & Glimcher LH The basic domain/leucine zipper protein hXBP-1 preferentially binds to and transactivates CRE-like sequences containing an ACGT core. Nucleic Acids Res 24, 1855–1864 (1996). [PubMed: 8657566]
40. Allan DS et al. An in vitro model of innate lymphoid cell function and differentiation. Mucosal Immunol 8, 340–351 (2015). [PubMed: 25138665]
41. Robertson MJ et al. Characterization of a cell line, NKL, derived from an aggressive human natural killer cell leukemia. Exp Hematol 24, 406–415 (1996). [PubMed: 8599969]
42. Frazier WR, Steiner N, Hou L, Dakshanamurthy S & Hurley CK Allelic variation in KIR2DL3 generates a KIR2DL2-like receptor with increased binding to its HLA-C ligand. Journal of immunology (Baltimore, Md. : 1950) 190, 6198–6208 (2013).
43. Foley B et al. The biology of NK cells and their receptors affects clinical outcomes after hematopoietic cell transplantation (HCT). Immunol Rev 258, 45–63 (2014). [PubMed: 24517425]
44. Ruggeri L et al. Effectiveness of donor natural killer cell alloreactivity in mismatched hematopoietic transplants. Science 295, 2097–2100 (2002). [PubMed: 11896281]
45. Molgora M et al. IL-1R8 is a checkpoint in NK cells regulating anti-tumour and anti-viral activity. Nature 551, 110–114 (2017). [PubMed: 29072292]
46. Bottcher JP et al. NK Cells Stimulate Recruitment of cDC1 into the Tumor Microenvironment Promoting Cancer Immune Control. Cell 172, 1022–1037 e1014 (2018). [PubMed: 29429633]
47. Siddiquey MNA, Zhang H, Nguyen CC, Domma AJ & Kamil JP The Human Cytomegalovirus Endoplasmic Reticulum-Resident Glycoprotein UL148 Activates the Unfolded Protein Response. J Virol 92 (2018).
48. Sun JC & Lanier LL Is There Natural Killer Cell Memory and Can It Be Harnessed by Vaccination? NK Cell Memory and Immunization Strategies against Infectious Diseases and Cancer. Cold Spring Harb Perspect Biol (2017).
49. Orange JS Natural killer cell deficiency. J Allergy Clin Immunol 132, 515–525 (2013). [PubMed: 23993353]
50. Vivier E, Ugolini S, Blaise D, Chabannon C & Brossay L Targeting natural killer cells and natural killer T cells in cancer. Nat Rev Immunol 12, 239–252 (2012). [PubMed: 22437937]
51. Barrow AD et al. Natural Killer Cells Control Tumor Growth by Sensing a Growth Factor. Cell 172, 534–548 e519 (2018). [PubMed: 29275861]
52. Ferrari de Andrade L et al. Antibody-mediated inhibition of MICA and MICB shedding promotes NK cell-driven tumor immunity. Science 359, 1537–1542 (2018). [PubMed: 29599246]
53. Adams NM et al. Transcription Factor IRF8 Orchestrates the Adaptive Natural Killer Cell Response. Immunity 48, 1172–1182 e1176 (2018). [PubMed: 29858012]
54. Andre P et al. Anti-NKG2A mAb Is a Checkpoint Inhibitor that Promotes Anti-tumor Immunity by Unleashing Both T and NK Cells. Cell 175, 1731–1743 e1713 (2018). [PubMed: 30503213]
55. van Montfoort N et al. NKG2A Blockade Potentiates CD8 T Cell Immunity Induced by Cancer Vaccines. Cell 175, 1744–1755 e1715 (2018). [PubMed: 30503208]
56. Barry KC et al. A natural killer-dendritic cell axis defines checkpoint therapy-responsive tumor microenvironments. Nat Med 24, 1178–1191 (2018). [PubMed: 29942093]

57. Rabacal W et al. Transcription factor KLF2 regulates homeostatic NK cell proliferation and survival. Proceedings of the National Academy of Sciences of the United States of America 113, 5370–5375 (2016). [PubMed: 27114551]
58. Wang Y et al. The IL-15-AKT-XBP1s signaling pathway contributes to effector functions and survival in human NK cells. Nature immunology 20, 10–17 (2019). [PubMed: 30538328]
59. Marcais A et al. The metabolic checkpoint kinase mTOR is essential for IL-15 signaling during the development and activation of NK cells. Nature immunology 15, 749–757 (2014). [PubMed: 24973821]
60. Yang C et al. mTORC1 and mTORC2 differentially promote natural killer cell development. Elife 7 (2018).
61. Zhao N et al. Pharmacological targeting of MYC-regulated IRE1/XBP1 pathway suppresses MYC-driven breast cancer. The Journal of clinical investigation 128, 1283–1299 (2018). [PubMed: 29480818]
62. Kortlever RM et al. Myc Cooperates with Ras by Programming Inflammation and Immune Suppression. Cell 171, 1301–1315 e1314 (2017). [PubMed: 29195074]
63. Chou C et al. c-Myc-induced transcription factor AP4 is required for host protection mediated by CD8+ T cells. Nature immunology 15, 884–893 (2014). [PubMed: 25029552]
64. Cichocki F et al. The transcription factor c-Myc enhances KIR gene transcription through direct binding to an upstream distal promoter element. Blood 113, 3245–3253 (2009). [PubMed: 18987359]
65. Zakiryanova GK et al. Alterations of oncogenes expression in NK cells in patients with cancer. Immun Inflamm Dis 5, 493–502 (2017). [PubMed: 28695716]

References (Methods-only)

66. Fodil-Cornu N et al. Ly49h-deficient C57BL/6 mice: a new mouse cytomegalovirus-susceptible model remains resistant to unrelated pathogens controlled by the NK gene complex. Journal of immunology (Baltimore, Md. : 1950) 181, 6394–6405 (2008).
67. Iwawaki T, Akai R, Yamanaka S & Kohno K Function of IRE1 alpha in the placenta is essential for placental development and embryonic viability. Proceedings of the National Academy of Sciences of the United States of America 106, 16657–16662 (2009). [PubMed: 19805353]
68. Trapnell C et al. Differential gene and transcript expression analysis of RNA-seq experiments with TopHat and Cufflinks. Nat Protoc 7, 562–578 (2012). [PubMed: 22383036]
69. Anders S, Pyl PT & Huber W HTSeq--a Python framework to work with high-throughput sequencing data. Bioinformatics 31, 166–169 (2015). [PubMed: 25260700]
70. Anders S & Huber W Differential expression analysis for sequence count data. Genome Biol 11, R106 (2010). [PubMed: 20979621]
71. Subramanian A et al. Gene set enrichment analysis: a knowledge-based approach for interpreting genome-wide expression profiles. Proceedings of the National Academy of Sciences of the United States of America 102, 15545–15550 (2005). [PubMed: 16199517]
72. Chen X et al. Integration of external signaling pathways with the core transcriptional network in embryonic stem cells. Cell 133, 1106–1117 (2008). [PubMed: 18555785]
73. Peinado H et al. Melanoma exosomes educate bone marrow progenitor cells toward a pro-metastatic phenotype through MET. Nat Med 18, 883–891 (2012). [PubMed: 22635005]

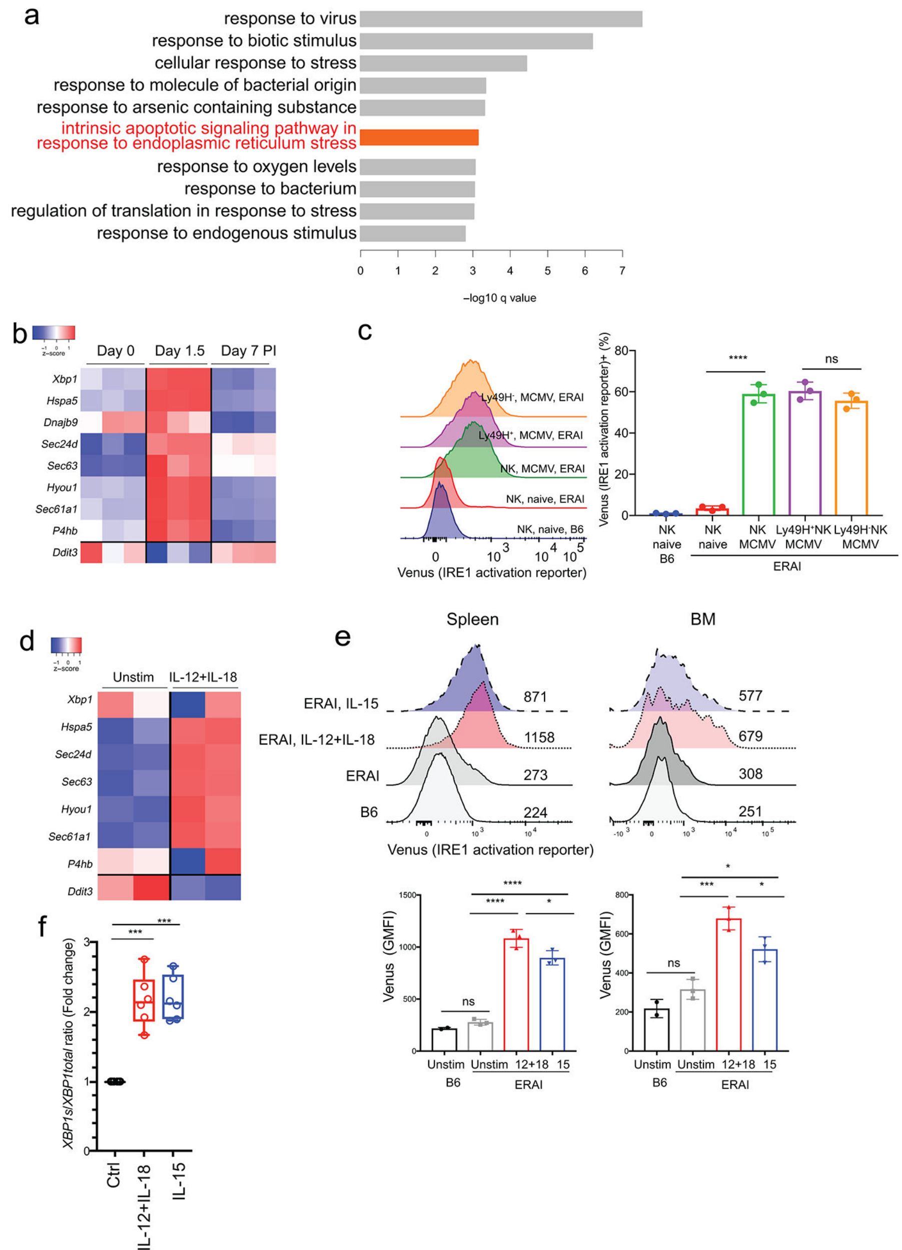

Figure 1. Induction of IRE1α-XBP1 UPR in mouse and human activated NK cells in *vitro* and *in vivo*.

(**a**) Gene ontology (GO) analysis of the top 500 differentially expressed genes in Ly49H$^+$ splenic NK cells harvested from either naïve or MCMV-infected mice day 1.5 post infection (PI). Top 10 GO clusters with the key word ‘stimulus’ were shown. n = 3 mice/group. (**b**) RNA-seq analysis showing the expression of canonical IRE1α-XBP1 target genes during a time course PI. (**c**) Flow cytometric analysis of Venus reporter expression in splenic NK cells from ERAI transgenic mice at day 2 PI. (**d**) RNA-seq analysis showing the expression of canonical IRE1α-XBP1 target genes in splenic NK cells harvested from WT mice and cultured either in the presence or absence of IL-12 and IL-18 for 16 hr (**GSE106138**). (**e**) Flow cytometric analysis of Venus reporter expression in sorting-purified splenic and BM

NK cells from ERAI transgenic mice following 16 hr culture in the presence or absence of IL-12 and IL-18, or IL-15. Each column (**b**, **d**) or symbol (**c**, **e**) represents an individual mouse. (**f**) Quantitative real-time PCR analysis of XBP1 splicing activity in sorted-purified human primary NK cells from PBMCs after 16 hrs culture in the presence or absence of IL-12 and IL-18, or IL-15. β-ACTIN was used as reference, and data are shown as fold change normalized to the unstimulated levels. n = 6 PBMC donors. Error bars represent mean with s.d. (**c**, **e**) or with minimal to maximal (**f**). Data were analyzed by one-way analysis of variance (ANOVA) with the Tukey post-test (**c**, **e**), or two-sided one sample *t*-test (**f**). *p<0.05, ***p<0.001, ****p<0.0001, ns = not significant. Data are representative of 3 (**c**, **e**) or 2 (**f**) independent experiments.

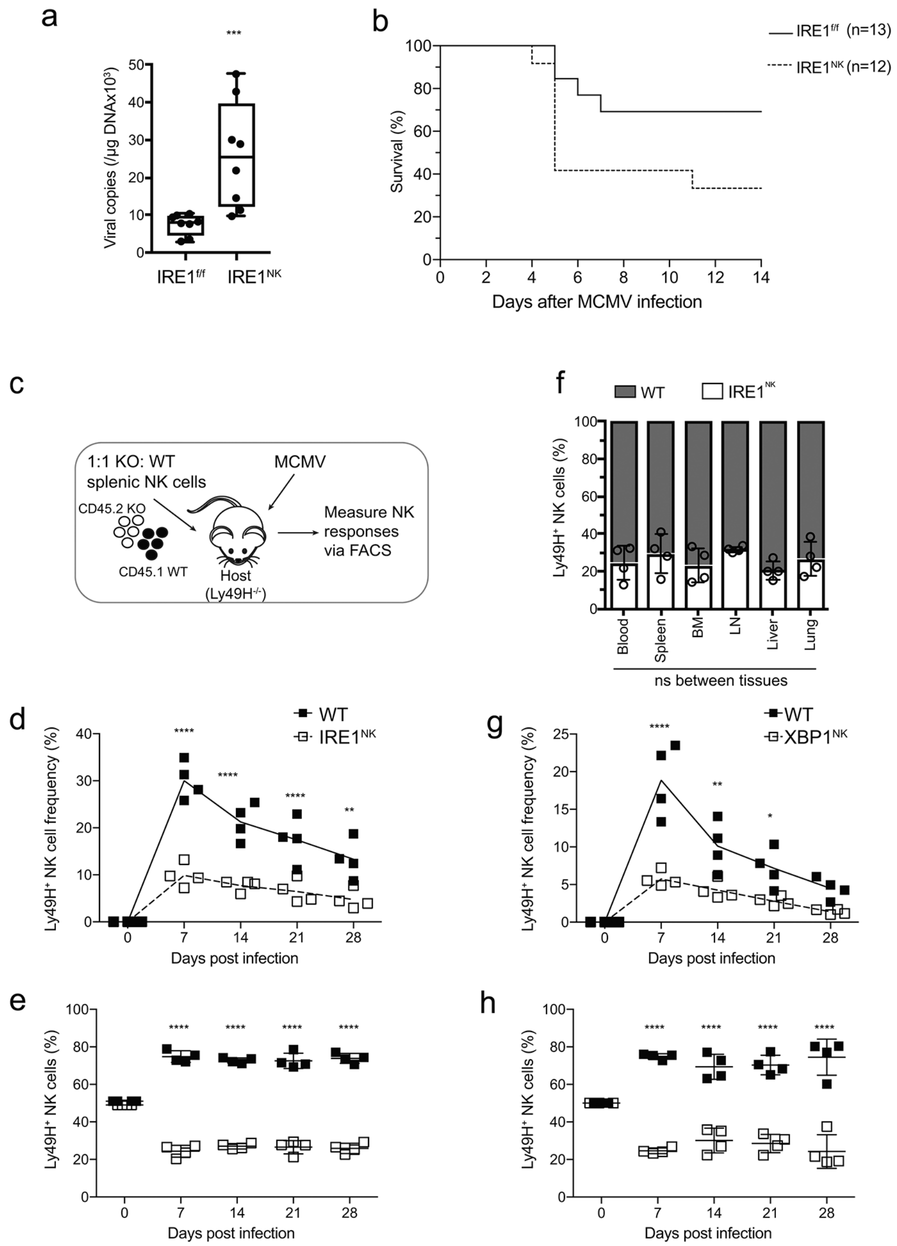

Figure 2. IRE1α is required for optimal protective antiviral NK cell responses.

(**a, b**) IRE1^{NK} and littermate control mice were infected with a lethal dose of MCMV. (**a**) Viral titers in the blood at day 4 PI. n = 8 mice/group. (**b**) Survival curve. n as indicated in the key. (**c**) Schematic of co-transfer experiments in **d**-**h**: Equal numbers of Ly49H$^+$ NK cells from WT (CD45.1) and knockout (KO; CD45.2) donors were co-transferred into recipient Ly49H-deficient mice 1 day before infection with MCMV. (**d**) Quantification of the percentage of transferred WT and IRE1^{NK} Ly49H$^+$ NK cells in peripheral blood at specified time points PI. Lines showed expansion kinetics by connecting mean values of adjacent time points in ggroup. (**e**) As in **d**, except showing the relative percentage within the transferred Ly49H$^+$ NK cells. (**f**) Relative percentages of transferred WT and IRE1^{NK} Ly49H$^+$ NK cells in various organs at day 8 (LN) or day 10 (all other tissues) PI. LN, lymph nodes. n = 4 recipient mice/column. **(g)** As in **d**, except the KO donors were XBP1^{NK}. (**h**) As in **e**, except the KO donors were XBP1^{NK}. n = 4 recipient mice (**d**, **e**, **g**. **h**). Error bars represent mean with minimal to maximal (**a**) or with s.d.(**e**, **f**, **h**). Data were analyzed by two tailed Mann-Whitney test (**a**), two-sided Log rank test (**b**, with p=0.0601), or two-way analysis of variance (ANOVA) with the Sidak post-test (**d-h**). *p<0.05, **p<0.01, ***p<0.001, ****p<0.0001, ns = not significant. Data are representative of 3 (**a**, **f, g, h**) or 4 (**d, e**) independent experiments, or pooled from 3 experiments (**b**).

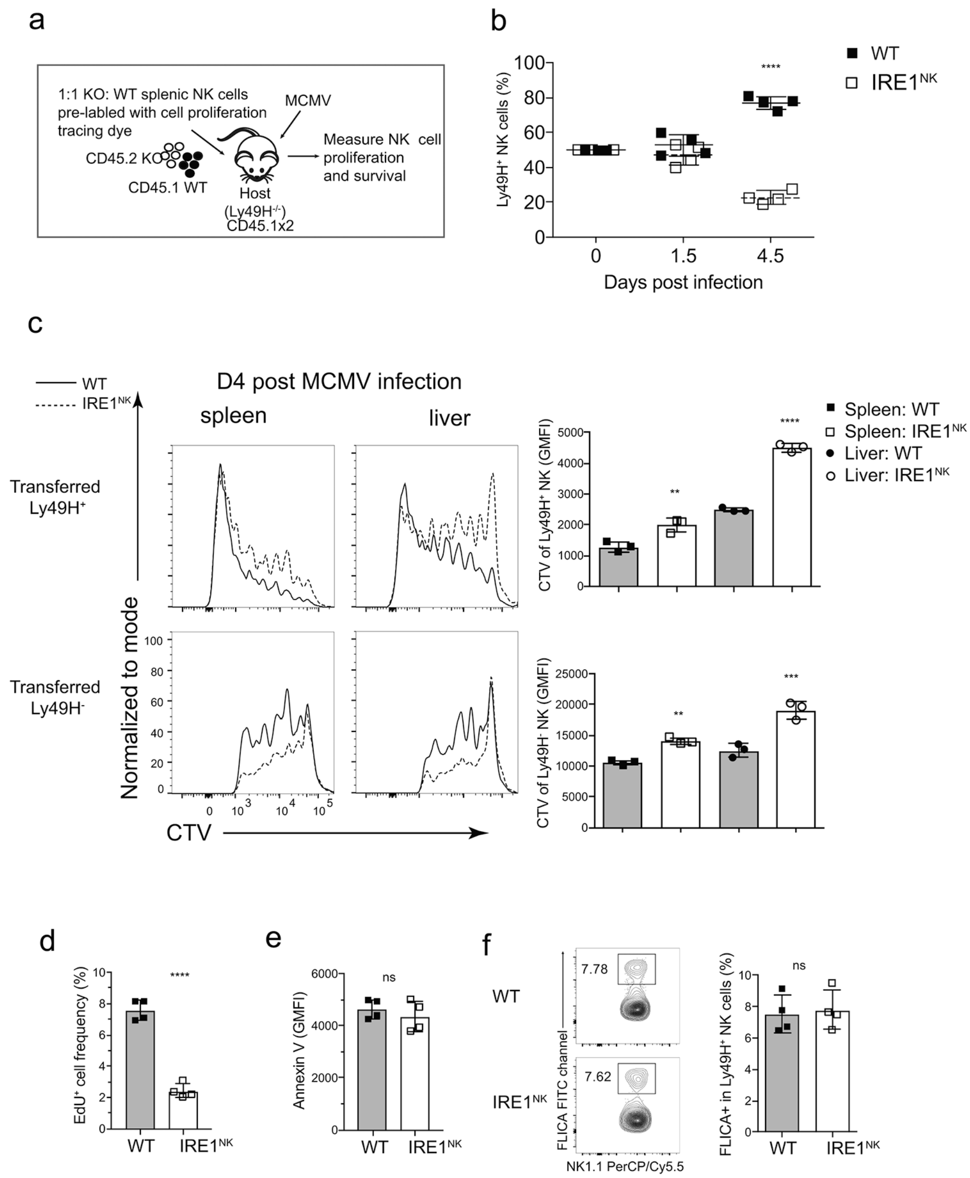

Figure 3. IRE1α-XBP1 controls infection-induced NK cell proliferation but not survival.

(**a**) Schematic of assays evaluating infection-driven NK cell proliferation and apoptosis in **b-f**. Equal numbers of Ly49H+ NK cells from WT (CD45.1) and IRE1^{NK} (CD45.2) donors were labelled with cell proliferation tracing dye CTV, and then co-transferred into recipient Ly49H-deficient mice 1 day before infection with MCMV. (**b**) Relative percentages of transferred WT and IRE1^{NK} Ly49H+ NK cells in the spleen of recipient Ly49H-deficient mice at specified time points PI. (**c**) Representative plots (left) and quantifications (right) of flow cytometric analysis showing CTV dilution of transferred WT and IRE1^{NK} Ly49H+ (responsive) and Ly49H− (bystander) NK cells in the spleen at day 4 PI. Flow cytometric analysis of EdU (**d**) and Annexin V (**e**) in co-transferred Ly49H+ NK cells at day 3.5 PI. EdU was injected intraperitoneally into mice 12 hr before measurement. (**f**) Representative flow cytometric plots (left) and quantifications (right) of percentage of FLICA+ cells in co-transferred Ly49H+ NK cells as in **d**. n = 4 mice/group for all experiments except n = 3 mice/group in **c**. All error bars represent mean with s.d.. **p<0.01, ***p<0.001, ****p<0.0001, ns = not significant. Data were analyzed by two-way analysis of variance (ANOVA) with the Sidak post-test (**b**), one-way analysis of variance (ANOVA) with the Tukey post-test (**c**), or two tailed unpaired Student's *t*-test (**d-f**). Data are representative of 3 (**b**, **c**, **f**) or 2 (**d**, **e**) independent experiments.

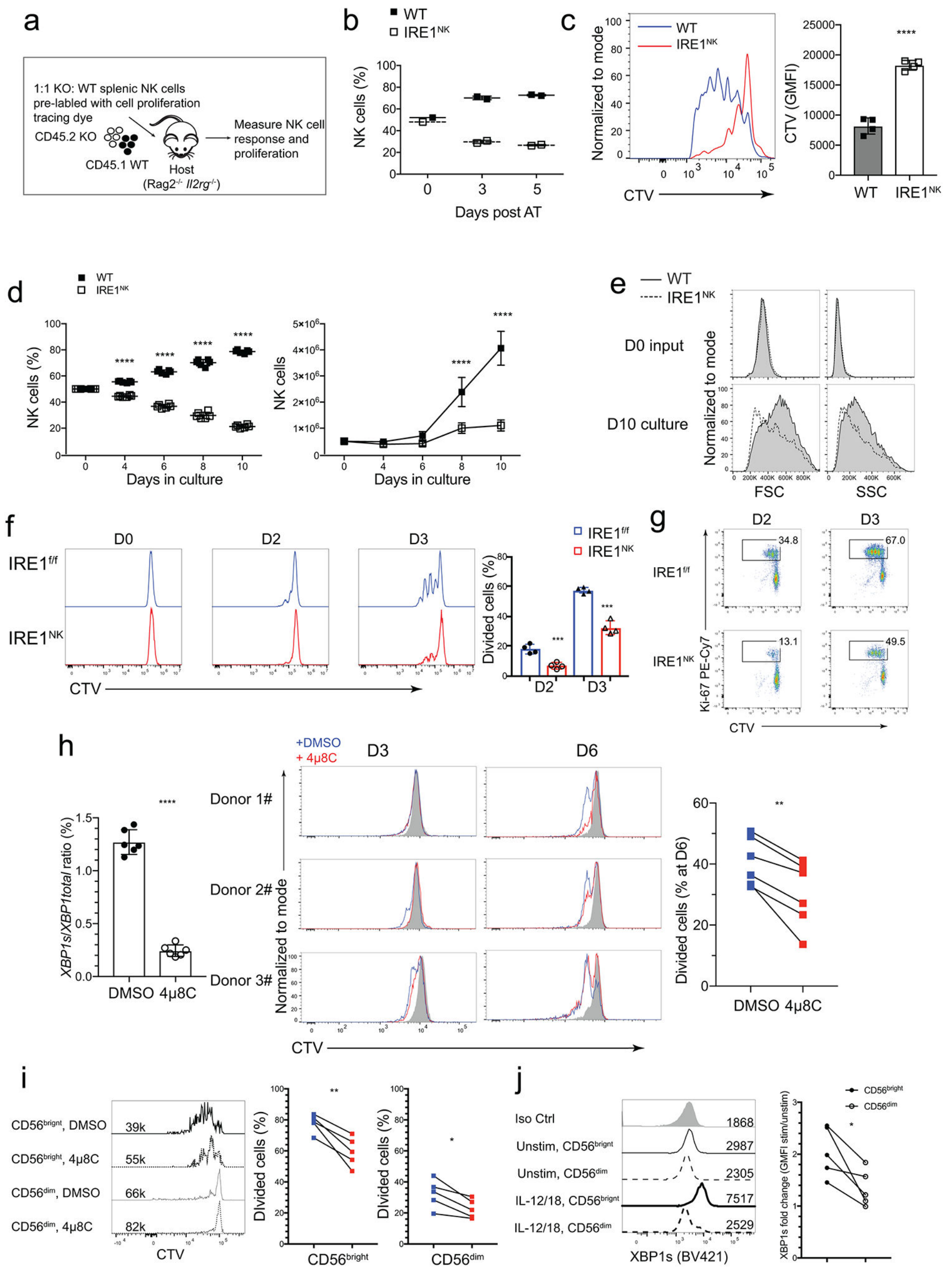

Figure 4. IRE1α-XBP1 supports NK homeostatic proliferation.

(**a**) Schematic of lymphopenia-induced homeostatic proliferation experiments in **b**, **c**. (**b**) Relative percentage of transferred WT and IRE1^{NK} cells in the spleen of *Rag2*$^{-/-}$ *Il2rg*$^{-/-}$ recipients at specified time points after transfer. (**c**) Representative flow cytometric plots and quantification of CTV dilution of transferred NK cells in the spleen of recipient mice at day 4 after transfer. (**d**) Relative percentages and absolute number of WT and IRE1^{NK} cells after co-incubation with IL-2 and IL-15. (**e**) Representative flow cytometric plots of FSC and SSC of cells in **d**. (**f**, **g**) IRE1^{NK} and IRE1$^{f/f}$ cells from littermates were pre-labeled with CTV and cultured with IL-2 and IL-15. Flow cytomemetic assays showing (**f**) CTV dilution and (**g**) Ki-67 levels at specified time points. (**h**) Human primary NK cells were cultured with

IL-2 and IL-15, in the presence or absence of the IRE1 inhibitor 4μ8C. (left) Quantitative real-time PCR analysis of *XBP1* splicing activity after 16 hr. β-ACTIN was used as reference. (middle) Flow cytometric analysis of CTV dilution at specified time points. Plots showed representative data derived from three PBMC donors. (right) Quantification of percentages of divided cells at day 6. (**i**) Flow cytometric analysis of CTV dilution as in **h**, except $CD56^{bright}$ and $CD56^{dim}$ cells were plotted separately. (**j**) Representative flow cytometric plots and quantification of XBP1s protein levels in $CD56^{bright}$ and $CD56^{dim}$ NK cells before and after 16 hr of cytokine stimulation. n = 2 mice/group in **b**. n = 4 mice/group in **c, f, g**. n = 3 mice/group (and 2 wells/mice for *ex vivo* culture) in **d**, **e**. n = 6, 5 and 5 PBMC donors in **h, i** and **j**. All error bars represent mean with s.d.. *p<0.05, **p<0.01, ***p<0.001, ****p<0.0001. Data were analyzed by two-tailed unpaired Student's *t*-test performed (**c**), two-way analysis of variance (ANOVA) with the Sidak post-test (**d**), one-way analysis of variance (ANOVA) with the Tukey post-test (**f**), or two-tailed paired Student's *t*-test (**h-j**). Data are representative of 3 (**b**, **c**) or 2 (**d-g**) independent experiments, or pooled from 2 independent experiments (**h-j**).

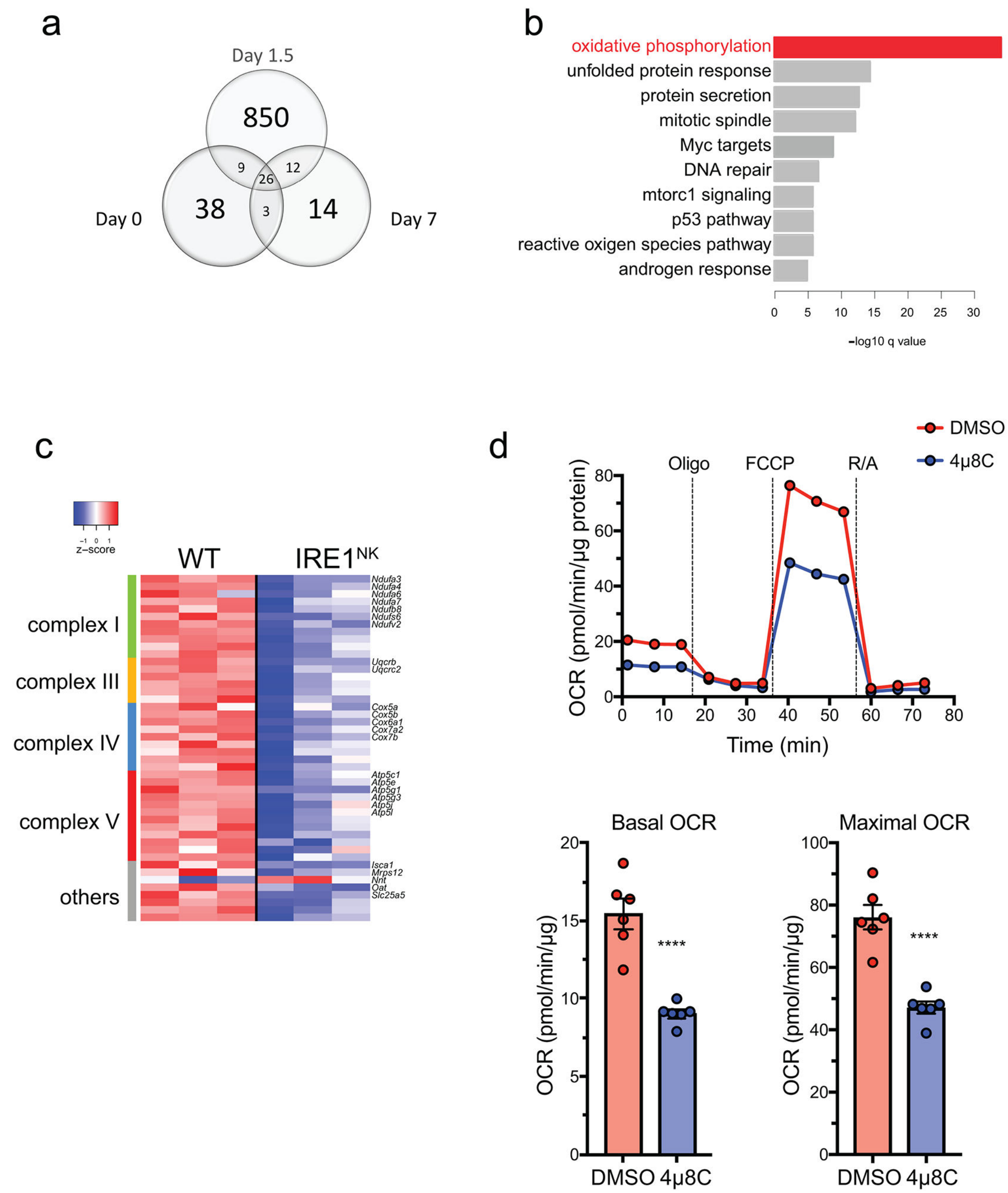

Figure 5. IRE1 supports NK cell OXPHOS and mitochondrial function.

(a) Venn diagram of RNA-seq analysis showing differentially expressed genes in IRE1^{NK} Ly49H^{+} NK cells compared to WT counterparts during infection with MCMV. Cells were harvested from IRE1^{NK} (CD45.2): WT (CD45.1) mixed BM chimeras at three time points: day 0, 1.5 and 7 PI. n = 3 mice/group (**b**) Top 10 enriched GSEA hallmark gene sets in RNA-seq analysis at day 1.5 PI as indicated in **a**. n = 3 mice/group. (**c**) The heat map of differentially expressed OXPHOS target genes in IRE1^{NK} versus WT NK cells at day 1.5 PI. Genes were clustered by functional annotation. c-Myc-regulated genes[35] are shown in black text on the right. (**d**) Analysis of NK cell oxygen consumption rate (OCR) to assess rates of OXPHOS and maximal respiration. Primary human NK cells isolated from PBMC were incubated with IL-12 and IL-18 for 16 hr, in the presence or absence of the IRE1α inhibitor 4μ8C (5 uM). Approximately 600, 000 cells were plated per well, and the data were normalized to total protein quantification. Oligo (Oligomycin, 1 μM), FCCP (carbonyl cyanide-p-(trifluoromethoxy) phenylhydrazone, 1 μM), R (rotenone, 0.5 μM) and A (antimycin, 0.5 μM). Representative plot in **d** shows data from one PBMC donor with each symbol representing mean measurement of three technical replicates. Quantification in **d** shows the combined data from three PBMC donors and two independent experiments; two-tailed unpaired Student's *t*-test was performed, with error bars representing mean with s.e.m. and ****$p<0.0001$.

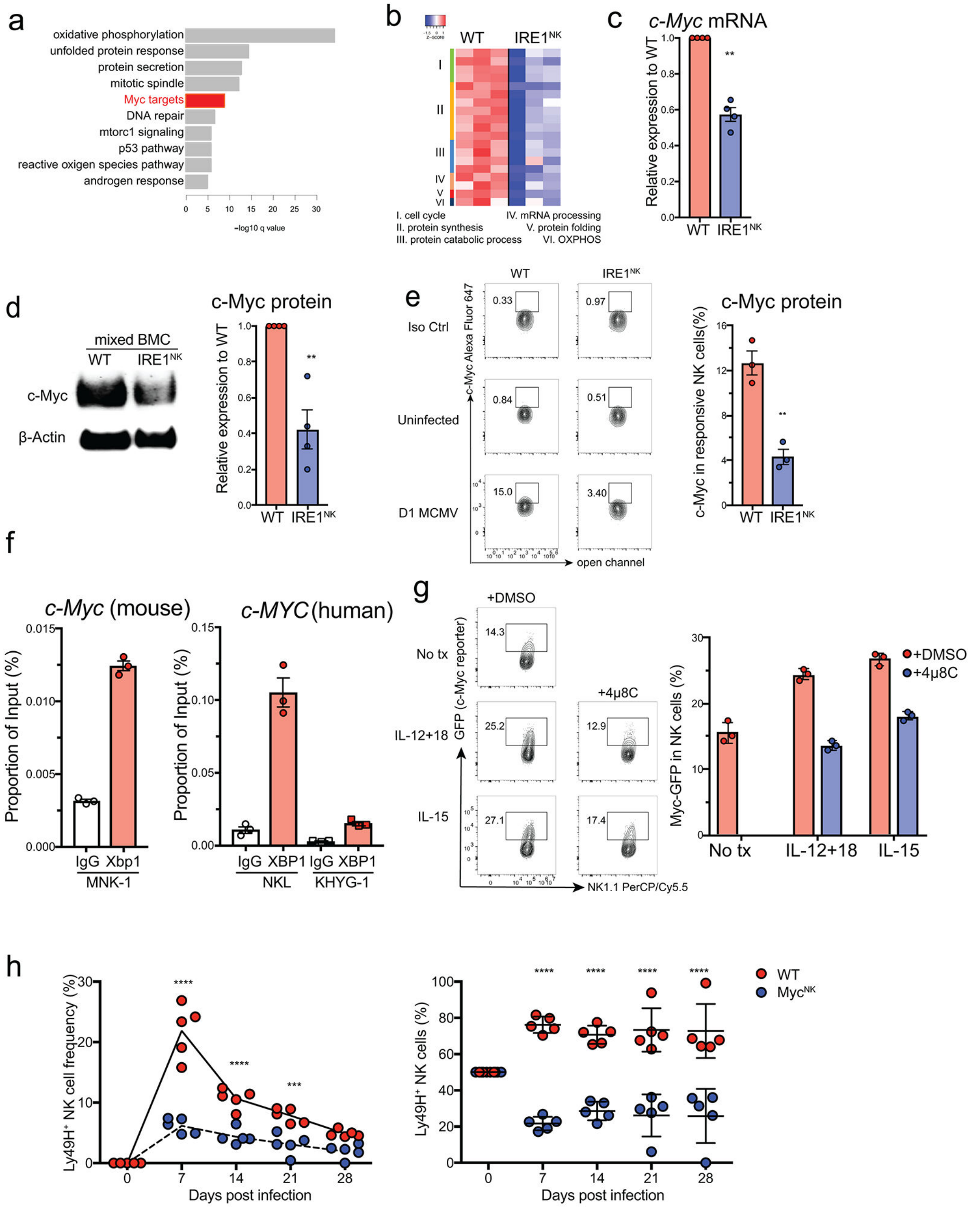

Figure 6. XBP1 promotes NK cell proliferation at least partially via direct regulation of c-Myc.

(**a**) Top 10 enriched GSEA gene clusters in RNA-seq analysis of IRE1^{NK} versus WT Ly49H^{+} splenic NK cells harvested from IRE1^{NK} (CD45.2): WT (CD45.1) mixed BM chimera mice day 1.5 PI. n = 3 BM chimera mice. (**b**) The heat map of differentially expressed canonical c-Myc target genes in IRE1^{NK} versus WT NK cells. Genes were clustered by functional annotation. Each column is a different mouse in group. (**c**) Quantitative real-time PCR analysis of *c-Myc* expression in transferred WT and IRE1^{NK} Ly49H^{+} NK cells in the spleen of recipient Ly49H-deficient mice at day 1 PI. Equal numbers of Ly49H^{+} NK cells from WT and KO donors were co-transferred into recipient Ly49H-deficient mice 1 day before infection. n = 4 recipient mice. (**d**) Representative immunoblot and quantification of c-Myc protein in IRE1^{NK} and WT NK cells sorted from the same mixed BM chimera mice at day 1.5 PI; quantification shows cumulative data from 4 mixed BM chimeras. (**e**) As in **c**, flow cytometric analysis of c-Myc expression in transferred WT and IRE1^{NK} Ly49H^{+} NK cells in the spleen of recipient Ly49H-deficient mice at day 1 PI. n = 3 recipient mice. (**f**) Chromatin immunoprecipitation assays using NK cell lines MNK-1 (mouse), NKL and KHYG-1 (human) to assess XBP1 binding to the *c-Myc* locus. Anti-XBP1s Ab was used and IgG was used as mock control. n = 3 technical replicates/group. (**g**) Representative flow cytometric plots and quantification of *c-Myc* reporter expression. Before assessment, splenic NK cells from c-Myc reporter mice (Myc^{GFP}) were treated with indicated cytokines for 16 hr, either in the presence or absence of the IRE1 inhibitor 4μ8C (5uM). n=3 wells/treatment in *ex vivo* culture. (**h**) (left) Percentages of transferred WT (CD45.1) and Myc^{NK} (CD45.2) Ly49H^{+} NK cells in peripheral blood (except the endpoint using spleen) at specified time points after infection with MCMV. Equal numbers of Ly49H^{+} NK cells from WT and Myc^{NK} donors were co-transferred into recipient Ly49H-deficient mice 1 day before infection. (right) The relative percentages within the transferred Ly49H^{+} NK cells. n = 5 recipient mice. All error bars represent mean with s.d.. **p<0.01, ****p<0.0001. Data were analyzed by two-tailed one sample t-test (**c**, **d**), two-tailed unpaired Student's t-test (**e**), or two-way analysis of variance (ANOVA) with the Sidak post-test (**h**). Data are representative of 3 (**c**, **e**, **g**) or 2 (**d**, **f**, **g**) independent experiments, or pooled from 2 experiments (**h**).

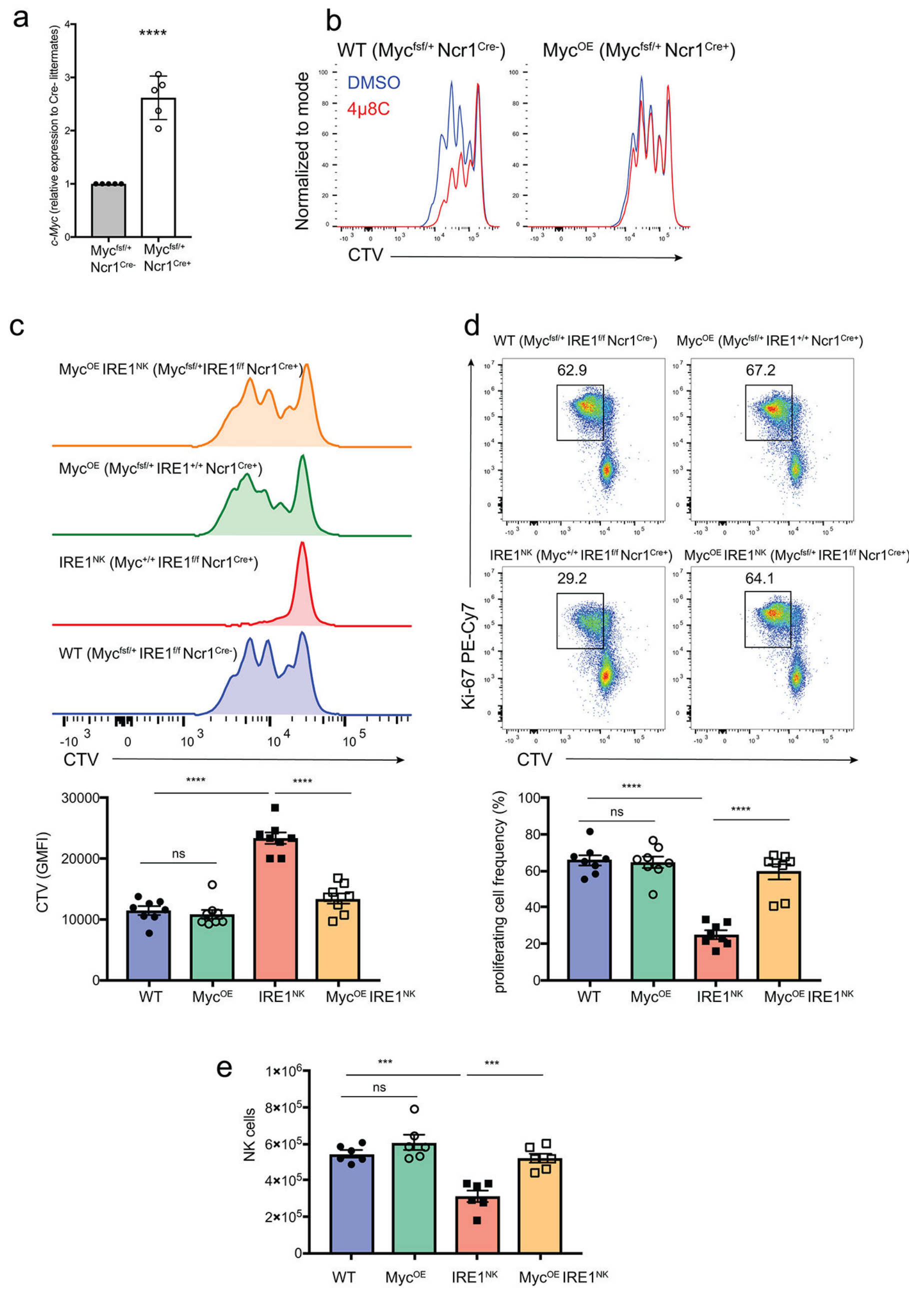

Figure 7. Restoration of c-Myc in the absence of IRE1 rescues the NK cell proliferation defect.
(**a**) Real-time PCR analysis of c-Myc mRNA in naïve NK cells from Myc^{OE} (Myc$^{fsf/+}$ Ncr1^{Cre+}) and littermate control (Myc$^{fsf/+}$Ncr1^{Cre-}) mice. (**b**) NK cells as in **a**, representative flow cytometric plots of CTV dilution after *ex vivo* culture with IL-2 and IL-15 for 3 days, in the presence or absence of IRE1α inhibitor 4μ8C (5 μM). (**c-e**) WT (Myc$^{fsf/+}$ IRE1$^{f/f}$ Ncr1^{Cre-}), IRE1^{NK} (Myc$^{+/+}$ IRE1$^{f/f}$ Ncr1^{Cre+}), Myc^{OE} (Myc$^{fsf/+}$ IRE1$^{+/+}$ Ncr1^{Cre+}) and Myc^{OE} IRE1^{NK} (Myc$^{fsf/+}$ IRE1$^{f/f}$ Ncr1^{Cre+}) NK cells were pre-labeled with CTV and cultured *ex vivo* with IL-2 and IL-15. (**c**) representative flow cytometric plots and quantification of CTV dilution at day 3, and (**d**) representative flow cytometric plots of Ki-67 levels and quantification of percentage of proliferating cells (defined as Ki-67+

CTV^{lo}) at day 3. (**e**) Absolute numbers of NK cells at day 6. n=5 mice/group in **a**, n = 2 mice/group in **b** and n= 4 mice/group in **c**-**e**. Technical duplicates in culture per mouse in **b**-**e**. All error bars represent mean with s.e.m.. ***p<0.001, ****p<0.0001. Data were analyzed by two-tailed one sample t-test (**a**), or one-way analysis of variance (ANOVA) with the Tukey post-test performed (**c**-**e**). Data are representative of 3 (**b**-**e)** independent experiments or pooled from 2 experiments (**a**).

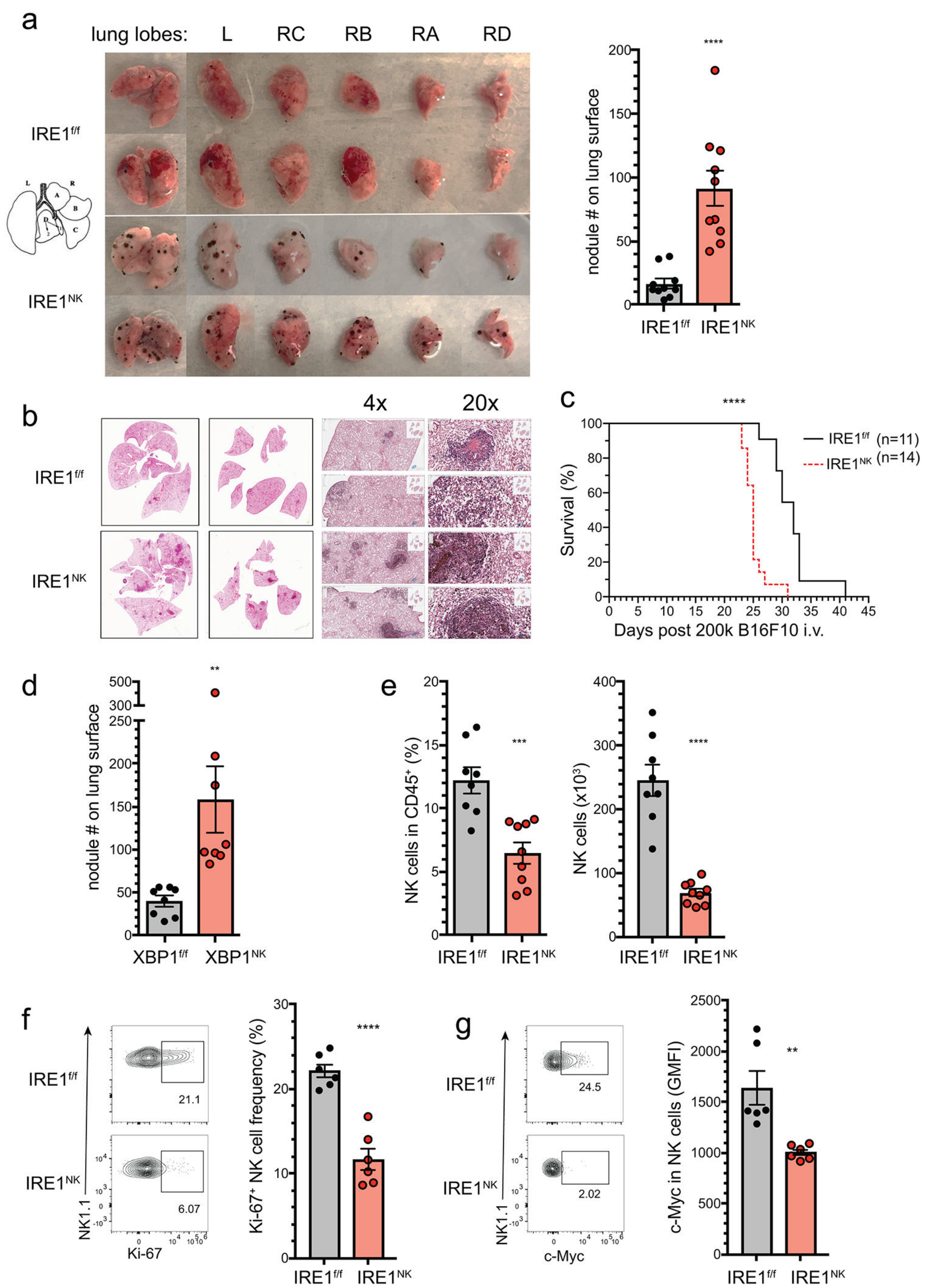

Figure 8. Intrinsic requirement of IRE1α/XBP1 for NK cell-mediated antitumor immunity.
(**a**) Gross morphology of lungs and individual lung lobes from IRE1$^{f/f}$ and IRE1^{NK} littermates at day 10 following intravenous injection of B16F10 melanoma. Quantification of total extrapulmonary metastatic nodules is shown on the right. n = 10 mice/group. (**b**) H&E microscopic analysis of lungs from IRE1$^{f/f}$ and IRE1^{NK} mice described in **a**. (**c**) Survival Curve of B16F10-innoculated IRE1$^{f/f}$ (n=11) and IRE1^{NK} (n=14) mice described in **a**. (**d**) Similar as in **a**, quantification of total extrapulmonary metastatic nodules from XBP1$^{f/f}$ and XBP1^{NK} littermates at day 20 following intravenous injection of B16F10 melanoma. n = 8

mice/group. (**e-g**) Flow cytometry analysis of lungs from B16F10 tumor-inoculated mice described in **a**. Graphs shown are (**e**) percentage of NK cells in total lymphocyte population and the absolute numbers (n = 8 for IRE1$^{f/f}$, n = 9 for IRE1^{NK}), (**f**) Ki-67 (n=6 mice/group) and (**g**) c-Myc expression (n = 6 mice/group) in lung-infiltrated NK cells. Each symbol is a different mouse (**a**, **d-g**). All error bars represent mean with s.e.m.. **p<0.01, ***p<0.001, ****p<0.0001. Data were analyzed by two-tailed Mann Whitney test (**a**, **d**, **e-g)**, or two-tailed Log-rank test (**c)**. Data are representative of 2 independnet experiments (**b**, **f**, **g**), or pooled from 3 (**a**) or 2 experiments (**c**-**e**).